AN ABSTRACT OF THE THESIS OF

John Buskirk for the degree of Master of Science in Nuclear Engineering presented on March 4, 2020.

Title: A Computational Investigation of Natural Circulation Effects on Heat Transfer Coefficient and Friction Factor.

Abstract approved: _____

Izabela Gutowska & Qiao Wu

The nuclear industry has shown a large interest in natural circulation driven passive cooling systems following the Fukushima nuclear accident. Despite this interest, there is no widely used heat transfer correlation or friction factor correlation developed for natural circulation driven flow. A CFD analysis including grid convergence testing using Fluent was performed to determine the applicable flow regimes for classic correlations. This analysis showed that classic heat transfer correlations cannot accurately predict local heat transfer unless heat flux is very small. When heat flux was high, heat transfer coefficients predicted by the Gnielinski

correlation were overpredicted by 40+%. Friction factors fell between laminar and turbulent values as expected, but neither correlation was accurate for any condition.

March 4, 2020

A Computational Investigation of Natural Circulation Effects on Heat Transfer Coefficient and Friction Factor

by

John Buskirk

A THESIS

submitted to

Oregon State University

in partial fulfillment of

the requirements for the

degree of

Master of Science

Presented March 4, 2020

Commencement June 2020

Master of Science thesis of John Buskirk presented on March 4, 2020

APPROVED:

Co-Major Professor, representing Nuclear Engineering

Co-Major Professor, representing Nuclear Engineering

Head of the School of Nuclear Science and Engineering

Dean of the Graduate School

I understand that my thesis will become part of the permanent collection of Oregon State University libraries. My signature below authorizes release of my thesis to any reader upon request.

John Buskirk, Author

ACKNOWLEDGEMENTS

I would like to expresses sincere appreciation to both Dr. Wu and Dr. Gutowska for their dedication to and support of this thesis. This thesis would not have been possible without their hard work and dedication. I would also like to thank Dr. Wu's research group for their help in improving my understanding of this and many other topics.

I would like to thank my friends in the NSE department for helping me both personally and academically during my time at OSU.

Lastly, I would like to that my parents for their support and encouragement throughout this process as well as my girlfriend who encourages me to be a better version of myself every day.

TABLE OF CONTENTS

Page

TABLE OF CONTENTS (Continued)

Page

TABLE OF CONTENTS (Continued)

Page

LIST OF FIGURES

Figure Page

LIST OF FIGURES (Continued)

Figure Page

LIST OF TABLES

Table Page

1. INTRODUCTION

1.1. Project Background and Motivation

Passive safety is a key component in many new reactor designs. One of the most prominent forms of passive safety is using natural convection to drive coolant flow inside reactors [35,36]. Despite the prominence of natural circulation in reactors, very little attention has been paid to the effects of this phenomenon under iso-flux conditions. Until this point, natural circulation driven pipe flow has been modelled and treated as similar or identical to pressure driven pipe flow for all situations. While this treatment may be valid in some scenarios, the fundamental equations governing friction factor and heat transfer coefficients suggest that differences in temperature and velocity profiles of natural circulation driven flow should have an impact under certain conditions.

Flow velocity profiles are directly proportional to friction factor and heat transfer as shown in equations 1 and 2:

$$f = \frac{2\tau_w}{\rho u^2} = \frac{\mu \frac{du}{dy}|_{wall}}{\frac{1}{2}\rho u^2} \quad (1)$$

$$h = \frac{\Delta T}{Q"} \quad (2)$$

Where $\frac{du}{dy}|_{wall}$ is defined as the slope of the axial velocity profile at the wall. This means that if the slope of velocity at the wall changes, the friction losses will also change. This can be seen by the difference in classical correlations for laminar and turbulent friction losses. Natural circulation profiles are distinctly different from pressure driven laminar and turbulent

profiles. Rough examples of all three profiles can be seen in figure 1. The most important portion of this figure is the slope of each line at the far right side (the wall). Currently, the majority of design work in the nuclear industry is done using correlations based off of laminar or turbulent flow conditions such as the Blasius solution, the Dittus Boelter correlation, or the Gnielinski correlation.

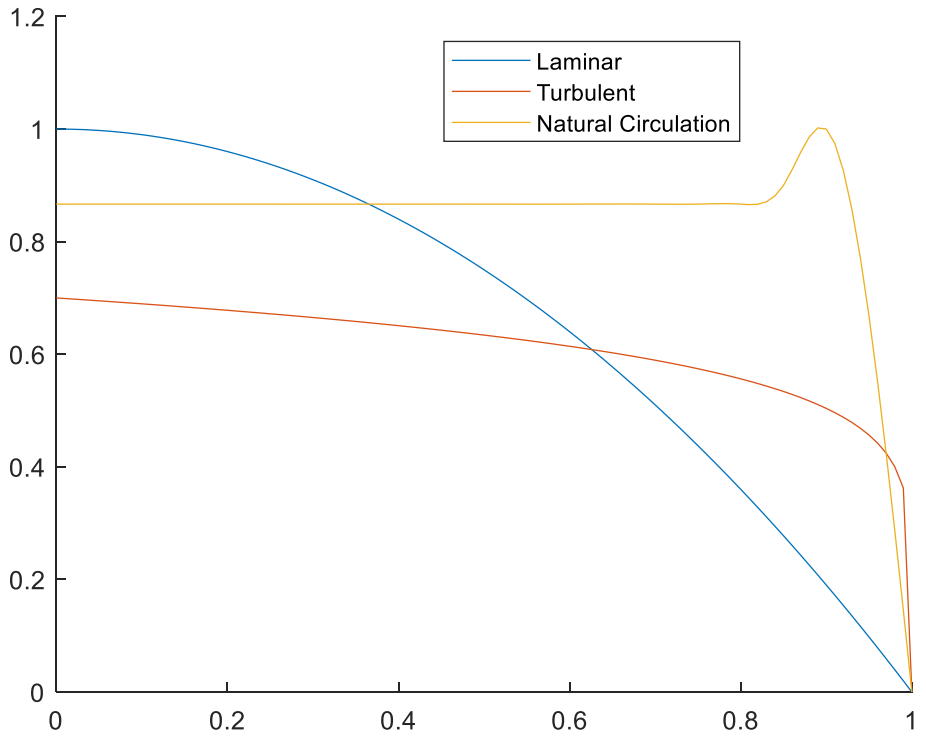

Figure 1: Representative flow profiles of varying regimes.

It is important to note that for natural circulation driven flow the peak velocity occurs near the wall while the peak occurs at the centerline for pressure driven flow. This wall peak occurs

due to the local change in density of the heated fluid near the wall. This change in density causes buoyant forces to accelerate the less dense fluid leading to a wall peak.

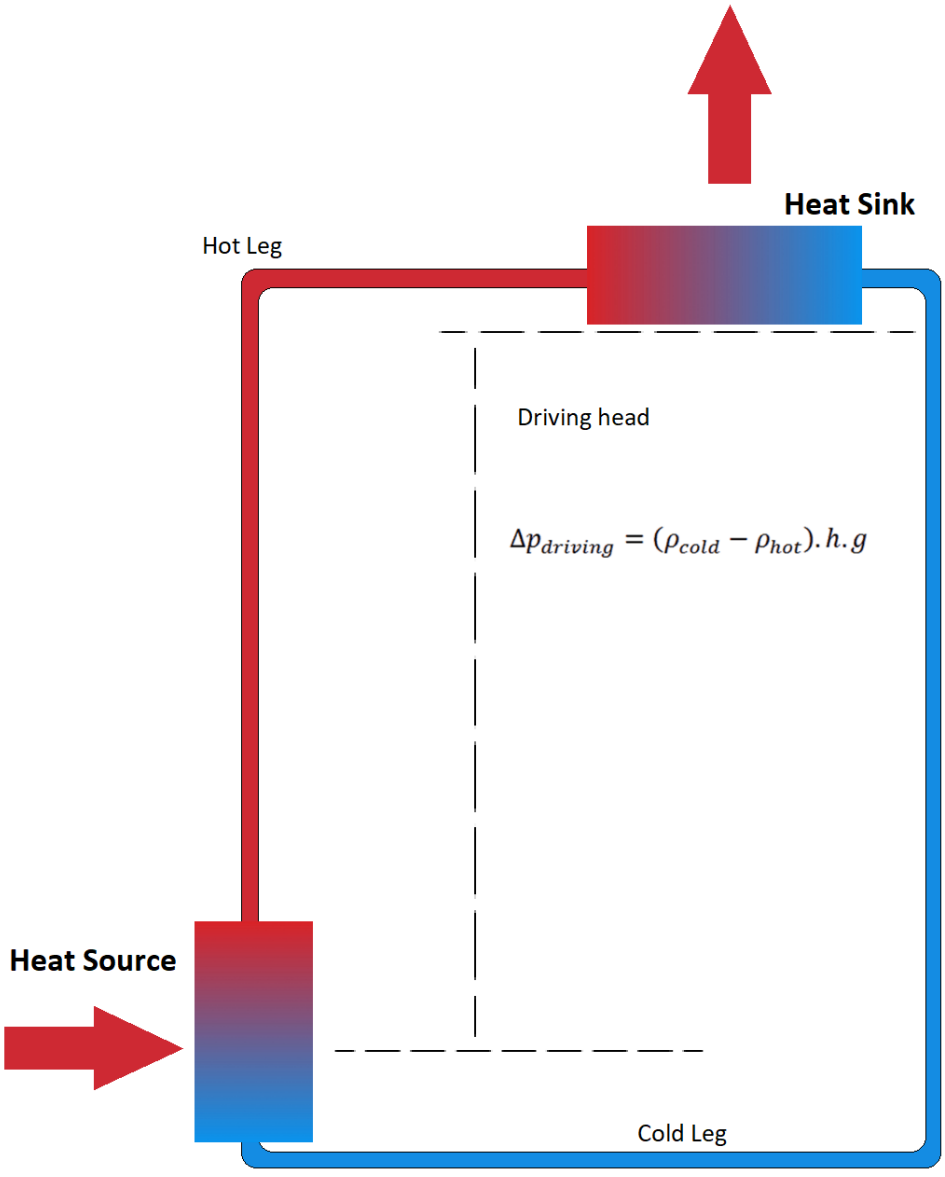

Figure 2: Simple natural circulation loop

A simple natural circulation loop (pictured in figure 2) consists of two vertical columns known as the hot and cold legs and two horizontal portions connecting the two legs. Heat is added to the loop at the bottom of the hot leg and rejected at the top of the cold leg. The traditional belief is that for a natural circulation driven loop to operate, it must be a certain height. This height then creates a large enough pressure difference between the hot and cold legs to drive flow through the loop. The pressure differential between hot and cold legs can be found using the difference in density between the two legs.

Due to the large variances in height required for this study, numerical methods are the most feasible method of performing this study accurately. To develop a physical experiment for this study, one would need to develop a precise method of measuring wall temperature along the heated portion of the wall. A detachable chimney of greatly varying height would also have to be included. Lastly an accurate, non-intrusive method of measuring near wall fluid velocity would be necessary. Measuring both heat and velocity at/near the wall without disrupting the flow are difficult and expensive tasks. As such, using a computational model to simulate these changes allows for a first feasibility study to be performed with much less time and cost.

1.2. Thesis Objectives

Both the forced and natural convection effects help to drive flow in a natural circulation loop. However, it is unknown under what conditions each drive dominates flow characteristics. This is especially important as when forced convection dominates, the flow should closely

resemble pressure driven flow; whereas when natural convection dominates, the flow should have wall peaks and much different friction factors/heat transfer coefficients. The primary objective of this research is to determine under what flow conditions classical correlations and equations accurately describe heat transfer and friction losses in vertical, natural circulation driven pipe flow using computational fluid dynamics software. A secondary goal is to develop a potential model to accurately describe these phenomena in regions where classical methods are inaccurate. These objectives are accomplished by developing temperature and velocity profiles. Heat transfer and friction factor are directly related to temperature and velocity gradients at the wall. Therefore, an accurate temperature and velocity profile are necessary to calculate the quantities of interest. These profiles will be developed using fluent. The determination of regions of applicability and potential development of more accurate models will result in a more accurate understanding of the dominance of loop or local drive and its effect on friction losses and heat transfer.

1.3. Assumptions and Limitations

Computational modeling of real-world phenomena requires assumptions to be made to develop the most accurate model possible. A brief description of major assumptions used in developing the computational model used are listed below:

- Natural circulation loops can be modeled as a single vertical pipe with an imposed pressure differential.

- Axisymmetric modeling can accurately capture relevant phenomena.
- Thermo-physical fluid properties such as the thermal expansion coefficient are assumed to be constant.
- The Boussinesq approximation can be applied.

The potentially most impactful assumption of this list is assuming constant properties other than density. This assumption keeps viscosity constant even though changing viscosity directly impacts friction factor. This assumption was made to ensure only the effects of changing buoyancy were captured as the effects of changing viscosity over a large temperature variance may wash out the buoyant effects. This allows for larger temperature variances to make the buoyant effects more pronounced/easily visible. However, this assumption decreases the physical accuracy of the model, especially for friction factor as friction factor is inherently proportional to viscosity. When comparing to physical scenarios, temperature differentials are also much lower, leading viscosity changes to be much more negligible. For the purposes of this study, the decreased accuracy in friction factor was determined to be less important than the increased buoyancy effects.

These assumptions create limitations for the validity of the computational model. A brief description of limitations is listed below:

- Minor and major friction losses are not accounted for outside of the simulation so effects of core geometry and other flow losses cannot be quantified.

- No physical test facility of this test was developed so assumptions made in fluent could affect the validity of this data.
- Due to the large quantity of data produced by a single simulation, quantities of interest are only evaluated at certain points and locations throughout the simulation.
- Fluent uses Reynolds averaged Navier-Stokes equations which limits the accuracy of the solution.
- The Boussinesq approximation is only applicable for small changes in temperature. Therefore, for results to be accurate, temperature differential must be minimized.

1.4. Outline

Chapter 1 presents a background information and brief overview of major topics as well as primary goals and objectives for this thesis.

Chapter 2 presents a review of relevant literature to more accurately understand concepts key to the validity of this thesis.

Chapter 3 provides the specifics of the computational model used in this thesis. This includes model geometry, mesh specifics, governing equations, initial and boundary conditions, and methodology for selecting cases.

Chapter 4 presents a grid independence study to assess the validity of the mesh and specify the uncertainty of the computational model.

Chapter 5 presents and discusses the heat transfer and friction factor results of the fluent simulation.

Chapter 6 discusses conclusions drawn from the results of this thesis as well as potential future work for improvement on this project.

2. LITERATURE REVIEW

2.1. Friction in Pipes

This section provides a brief history of the friction factor as well as its relation to shear stress at the wall. The history begins with the presentation of the Weisbach equation and continues on to the differentiation between laminar and turbulent flow. The history concludes with the development of the Rouse and Moody diagrams followed by a brief discussion of the correlation of the friction factor to shear stress at the wall.

2.1.1 The Weisbach Equation

Determining friction losses in pipe flow is an important step in any fluid system. In an effort to accurately characterize these losses, Julius Weisbach proposed equation 3 in 1845 [1].

$$h_l = \frac{fL}{D}\frac{V^2}{2g} \tag{3}$$

Where $D = Pipe\ Diameter, L = Pipe\ Length, f = friction\ factor, g = Gravity, V = velocity, and\ h_l = head\ (friction)\ losses$. It is important to note that Weisbach defined friction factor as

$$f = \alpha + \frac{\beta}{\sqrt{V}} \tag{4}$$

Where $\alpha\ and\ \beta$ are coefficients based on pipe diameter and wall material. This equation was quickly accepted as the standard globally, excluding France that used the Prony equation (equation 5).

$$h_l = \frac{L}{D}(aV + bV^2) \tag{5}$$

One key difference between the Prony and Weisbach equations is the Prony equation does not contain any dependence on wall roughness while Weisbach does (wall material). However, prior to the prevalence of computers and the slide rule, the Prony equation required six (or four if standard lower order terms are neglected) mathematical operations compared to the eight required for the Weisbach equation [2]. Despite friction factor being introduced in 1845, the modern definition of the term took over 100 years to be fully defined.

2.1.2 Laminar and Turbulent Effects

While Weisbach was developing his equation, Jean Poiseuille and Gotthilf Hagen independently determined that losses due to friction for low velocity flow in tubes could be determined using equations of the form [3,4]

$$h_l = \frac{64}{\rho} * (aT + bT^2) * \frac{L}{D^2}\frac{V}{2g} \quad (6)$$

$\frac{1}{\rho}(aT + bT^2)$ can be replaced with ν presenting the equation in modern terms as

$$h_l = 64\nu\frac{L}{D^2}\frac{V}{2g} \quad (7)$$

It is important to note that this relationship was determined solely experimentally as an analytical derivation of laminar flow would not be completed for another 20 years [5].

A few years before the analytical derivation of laminar flow was completed, Henry Darcy published an updated form of the Prony equation with added coefficients that included the effects of pipe roughness (although it was not known at that time that roughness was the parameter of interest) [6]. This relation to pipe roughness is why "f" is commonly referred to as the Darcy friction factor. Darcy noted that in low-flow in small pipes the velocity should increase proportionally with the gradient. In a future publication Darcy explicitly showed that his proposed form of the Prony equation reduced to Poiseuille's equation for low-flow in small pipes [7].

Roughly two decades later J.T. Fanning published tables of friction factor values for varying pipe materials, sizes and flow rates for use in the Weisbach equation [8]. These tables were obtained from a variety of American, English, French, and German sources and allowed engineers and designers to easily use the Weisbach equation by reducing the number of math operations required to solve to the same as the Prony. It is important to note that Fanning

used the hydraulic radius instead of pipe diameter leading to a factor of ¼ when comparing the Fanning and Darcy friction factors.

The next advancement occurred when Osbourne Reynolds published the transition point for laminar to turbulent flow in 1883 [9]. This was the first presentation of the Reynolds number,

$$Re = \frac{VD}{\nu} \tag{8}$$

By combining the Reynolds number with Poiseuille's equation (equation 7)) the currently used relation for laminar pipe flow (equation 9) can easily be obtained.

$$f = \frac{64}{Re} \tag{9}$$

This equation was widely used by the early 1900s but no specific source could be found for the first derivation.

Following Darcy's adaption of the Prony equation, no more advancements in the quantification of the turbulent friction factor were made until Blasius applied a similarity solution in 1913 [10]. Combining this approach with experimental data for smooth pipes led to the development of the Blasius formula shown in equation 10.

$$f = \frac{0.3614}{RE^{1/4}} \tag{10}$$

This was then improved on by Prandtl and Von Karman to the currently used form

$$\frac{1}{\sqrt{f}} = 2\log\left(Re\sqrt{f}\right) - 0.08 \tag{11}$$

Next Prandtl, Von Karman, Blasius, and Nikuradse developed friction factor correlations for the fully turbulent region. Equation 12 developed by Von Karman in 1930 and confirmed by Nikuradse in 1933 was the result of this work [11,12].

$$\frac{1}{\sqrt{f}} = 1.14 - 2\log\left(\frac{\epsilon}{D}\right) \tag{12}$$

The last region of turbulent flow to be characterized was the transition region. This region was finally characterized for commercial use by White in 1939 with equation 13 [7].

$$\frac{1}{\sqrt{f}} = 1.14 - 2\log\left(\frac{\epsilon}{D} + \frac{9.35}{Re\sqrt{f}}\right) \tag{13}$$

2.1.3 The Rouse and Moody Diagrams

Now that the friction factor had been accurately defined for essentially all pipe sizes, roughnesses, and flow rates by equations 9, 11, 12, and 13, the equations had to be converted into a useful form. This was first accomplished by Hunter Rouse in the early 1940s with the Rouse Diagram (figure 3). This diagram combined all four equations into a set of curves as well as defined a set transition point from transitional to turbulent flow [7]. During a

presentation of the diagram, Lewis Moody thought of a more conventional method of displaying the chart and developed the now widely used Moody Diagram shown in figure 4.

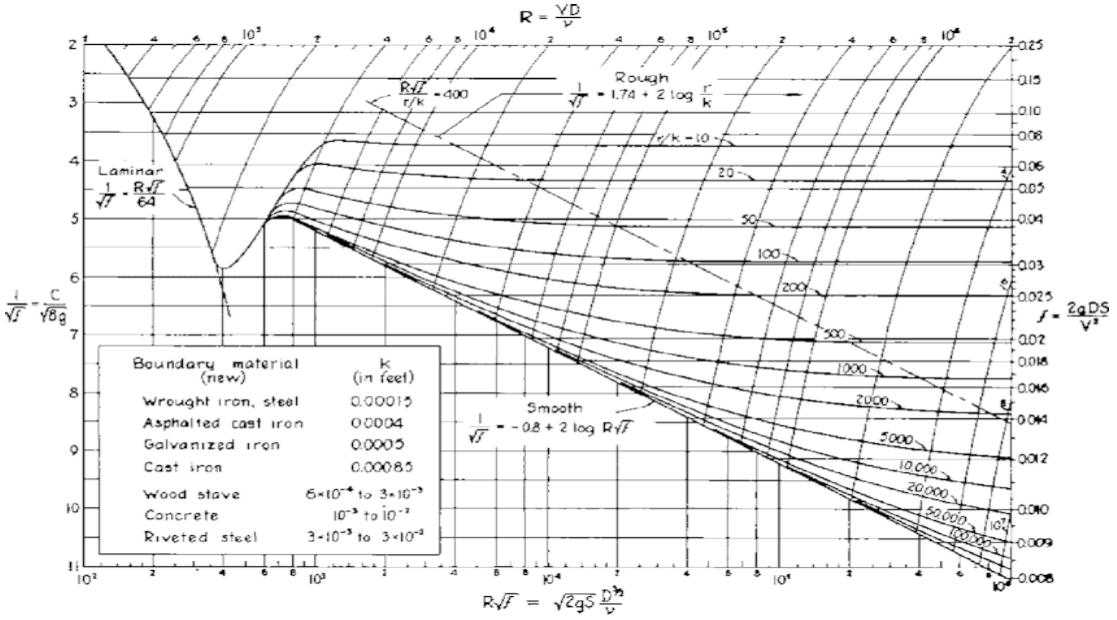

Figure 3: Rouse Diagram- Developed by Hunter Rouse for determination of friction factor [7]

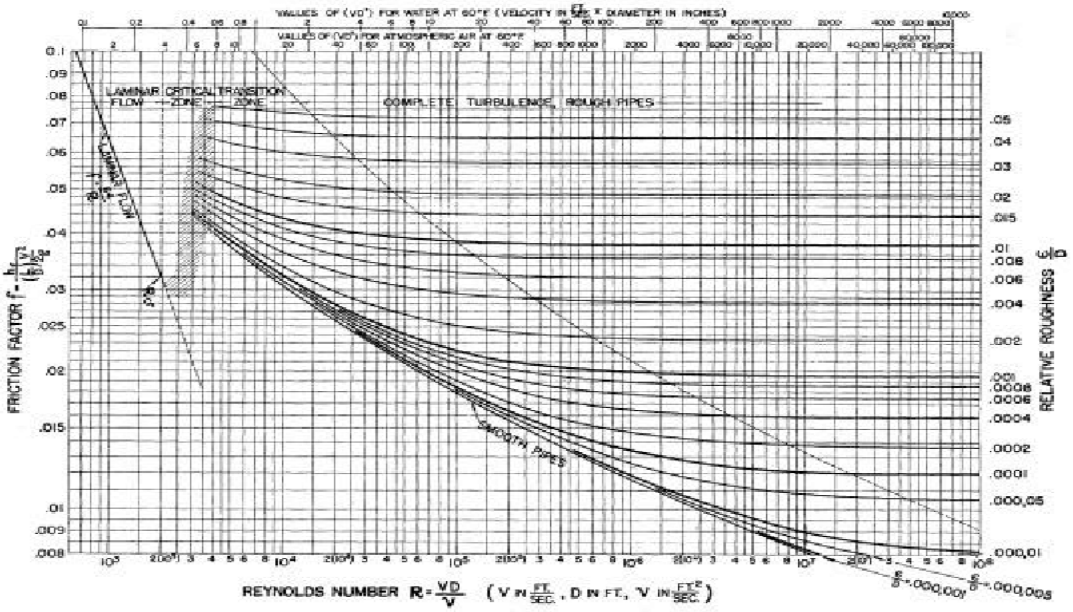

Figure 4: Moody Diagram for calculating friction factor in pipe flow [7]

2.1.4 Friction factor and Shear Stress

While the relationship between friction factor and shear stress at the wall may not be initially apparent when observing the Darcy-Weisbach equation, the relation between the two quantities becomes readily apparent with some algebra. The Darcy friction factor can be defined as [13]

$$f = \frac{\Delta P * 2(\frac{D}{L})}{\rho v^2} \tag{14}$$

Comparing this with the definition for wall shear stress [14]

$$\tau_w = \frac{\Delta P}{L} * \frac{D}{4} \tag{15}$$

It is apparent that both quantities are dependent upon ΔP. Rearranging the equations and substituting then yields

$$f = \frac{8\tau_w}{\rho v^2} \tag{16}$$

Equation 16 clearly defines the relationship between friction factor and shear stress at the wall. Note that the Fanning friction factor is more commonly used in application and, as previously discussed, is one fourth the Darcy friction factor as shown in equation 17.

$$f = \frac{2\tau_w}{\rho v^2} = \frac{2\left(\mu \frac{dU}{dy}|_{wall}\right)}{\rho v^2} \tag{17}$$

2.2. Heat Transfer Coefficients

This section discusses a variety of heat transfer correlations for one-phase forced laminar/turbulent internal flow and their origins/derivations. The discussion begins with an overview of non-dimensional numbers of interest followed by a brief discussion of the Reynolds and Colburn analogies. The discussion continues with laminar Nusselt numbers and turbulent correlations. This section concludes with factors that affect heat transfer other than flow regime.

2.2.1 Non-Dimensional Numbers of Interest

When discussing heat transfer, it is important to discuss non-dimensional numbers of interest and their meanings. This is important as all correlations discussed in the upcoming sections depend on a variety of non-dimensional numbers. All numbers will be presented as a ratio of two phenomena and a corresponding equation. A primary use/application is also included for each number.

2.2.1.1 Reynolds Number

$$Re = \frac{VD}{\nu}$$

In the previous sections, the Reynolds number was introduced as the defining number for transition from laminar to turbulent flow. This transition occurs between Re=2000 and

Re=4000 [7]. Another description of the Reynold's number is the ratio of inertial and viscous forces.

2.2.1.2 Prandtl Number

$$Pr = \frac{\nu}{\alpha} = \frac{c_p \mu}{k}$$

Where $\alpha = thermal\ diffusivity, c_p = specific\ heat, \mu = dynamic\ viscosity, and\ k = thermal\ conductivity$. The Prandtl number is the ratio of viscous and thermal diffusion rates. This means the Prandtl number can be used to compare the growth rate of the momentum and thermal boundary layers. Small Prandtl numbers (PR<<1) correspond to the thermal boundary layer dominating and large Prandtl numbers (PR>>1) correspond to domination by the momentum boundary layer.

2.2.1.3 Grashof Number

$$Gr = \frac{g\beta\Delta T L^3}{\nu^2}\ or\ \frac{g\beta\Delta T D^3}{\nu^2}$$

Where $g = gravity\ const., \beta = thermal\ expansion\ coefficient, \& \Delta T = temperature\ difference\ between\ the\ surface\ and\ free\ stream.$ The Grashof number is the ratio of buoyant and viscous forces [13]. The Grashof number is used similarly to the Reynolds number in that it distinguishes the transition from laminar to turbulent flow in natural convection. In vertical pipes, this transition occurs when $2.54 * 10^8 \leq Gr \leq 1.07 * 10^9$ [15].

2.2.1.4 Nusselt Number

$$Nu = \frac{hL}{k}$$

Where $h = convective\ heat\ transfer\ coefficient\ and\ k = thermal\ conductivity$. The Nusselt number is arguably the most important non-dimensional number for heat transfer as it is the ratio of convective and conductive heat transfer. The Nusselt number is generally used to determine the convective heat transfer coefficient (HTC). This is accomplished using one of the many developed correlations to solve for the Nusselt number and then use the definition of the Nusselt number to solve for the convective HTC. A variety of these correlations will be discussed in sections 2.2.3,2.2.4, and 2.3.

2.2.1.5 Rayleigh Number

$$Ra = \frac{g\beta\Delta TL^3}{\nu\alpha} = Gr * Pr$$

The Rayleigh number is used to compare the rate of thermal transport by diffusion with the rate of thermal transport by convection [15]. Therefore, there is a critical number for each fluid at which fluid will begin to move without any forced convective forces [13]. Below this critical number, heat is transferred only via conduction/diffusion whereas above this critical number, heat is transferred by both conduction and natural convection [16].

2.2.1.6 Richardson Number

$$Ri = \frac{g\beta\Delta TL}{V^2} = \frac{Gr}{Re^2}$$

The Richardson number compares the importance of natural and forced convection. This causes the Richardson number to be used to determine when effects of natural or forced convection can be neglected. The general rule used for determination of which effects must be considered is [17]:

$$When\ Ri < 0.3\ neglect\ forced\ convection$$

$$When\ 0.3 < Ri < 16\ Consider\ both\ forced\ and\ natural\ convection$$

$$When\ R > 16\ neglect\ free\ convection$$

2.2.2 Reynolds and Colburn Analogies

When observing diffusion equations for momentum and heat, the two equations appear remarkably similar. Reynolds was the first to notice this and developed an analogy between turbulent momentum and heat transfer known as the Reynolds analogy [18]. The Reynolds analogy relies on the assumption that heat flux and momentum flux are analogous. This assumption is validated as both quantities depend largely on turbulent eddies in the system [18]. By making this assumption Reynolds was able to develop the final form of his analogy presented in equation 18.

$$\frac{f}{2} = \frac{h}{c_p G} = \frac{\mathrm{K}'}{\mathrm{V_{av}}} \tag{18}$$

For laminar flow, this analogy can be reduced and manipulated to take the form [19]:

$$Re\frac{f}{2} = Nu = Sh \tag{19}$$

It is important to note that these equations are only valid when the Prandtl number is close to one and no form drag is present [19]. Also note that equations 18 and 19 are presented in the form $Momentum = Heat = Mass$ and that "Sh" is the Sherwood number, an important nondimensional number in mass transfer. For the purposes of this thesis only momentum and heat need be considered so the mass term will not be discussed.

Many improvements and adaptations of the Reynolds analogy have been developed and the most successful of these is the Chilton-Colburn analogy presented in equation 20.

$$Re\frac{f}{2} = Nu * Pr^{-\frac{1}{3}} \tag{20}$$

This analogy accurately includes the effects of varying Prandtl number. The range of applicability of this analogy is disputed in literature but conservatively is 0.7<Pr<60 [18,19]. When Pr=1 the Chilton-Colburn analogy reduces directly to the Reynolds analogy. These two analogies allow for quick calculation of heat transfer coefficients or friction factors if the other quantity is known.

2.2.3 Laminar Nusselt Numbers

Nusselt numbers are commonly used to determine convective heat transfer coefficients for pipe flow [20]. The reasoning for this can be seen when looking at the definition of the Nusselt number, $Nu = \frac{hL}{k}$. For any given setup, "k" and "l" are solely dependent upon material properties and setup. However, "h" is much more difficult to define. As such, the most accurate method of determining "h" is to apply an analytical solution or derived correlation for the Nusselt number.

For laminar pipe flow, an analytical solution can be obtained depending on geometry and heating profile [21]. The full derivation for these Nusselt numbers is a long, involved process that will not be completed in this thesis. However, the most applicable laminar Nusselt numbers are included here for reference. For circular pipes with constant heat flux or constant temperature, the laminar Nusselt numbers are 4.36 and 3.66 respectively [22].

2.2.4 Turbulent Correlations

An analytical solution for the Nusselt number in turbulent flow has not yet been determined. Instead, engineers rely on a variety of empirically derived correlations to accurately determine the Nusselt number in turbulent flow. The most prominently used of these correlations are the Dittus-Boelter, Sieder-Tate, and Gnielinski correlations [20].

2.2.4.1 Dittus-Boelter Equation

$$Nu_D = 0.023 Re_D^{\frac{4}{5}} Pr^n$$

$$n = 0.3 \; for \; cooling \; and \; n = 0.4 \; for \; heating$$

The most commonly used turbulent correlation is the Dittus-Boelter equation, proposed by Dittus and Boelter in 1930 [23]. This is mostly due to the simplicity of the correlation. The Dittus-Boelter equation is applicable for flow in smooth tubes with $0.6 < Pr < 160$ & $Re_D > 10{,}000$ fully developed flow. This correlation loses accuracy when large differences between the bulk and wall fluid temperatures exist. This loss of accuracy occurs due to the changing fluid properties not being accounted for.

2.2.4.2 Sieder-Tate Correlation

$$Nu_D = 0.023 Re_D^{\frac{4}{5}} Pr^{\frac{1}{3}} \left(\frac{\mu}{\mu_s}\right)^{0.14}$$

The Sieder-Tate correlation is nearly identical to the Dittus-Boelter equation except it includes a correction factor that takes into account the change in viscosity due to temperature variations in the fluid [20]. The inclusion of this correction factor makes Seider-Tate much more accurate for flows with large temperature changes and much higher Prandtl numbers (PR<16700) [24]. While this change is seemingly minor, it drastically increases computational time over Dittus-Boelter. This increase occurs because Sieder-Tate must be solved iteratively as the viscosity correction factor changes with changing Nusselt number. This increase in

complexity leads to Sieder-Tate being generally used only when Dittus-Boelter becomes inaccurate [20].

2.2.4.3 Gnielinski Correlation

$$Nu_D = \frac{\left(\frac{f}{8}\right)(Re_D - 1000)Pr}{1 + 12.7\left(\frac{f}{8}\right)^{0.5}\left(Pr^{\frac{2}{3}} - 1\right)}$$

While the Dittus-Boelter and Sieder-Tate correlations are generally accurate enough, they can lead to errors as high as 25% in some cases [16]. The Gnielinski correlation was developed in 1975 to correct these errors and improve the range of applicability [25]. This correlation is applicable for $0.5 < Pr < 2000$ & $3000 < Re < 500{,}000$. The most important part of this increase in applicability is the lowering of the Reynolds number into the transition region as no other widely used correlation is applicable in this region. Despite the improved accuracy, the Gnielinski correlation is not widely used outside of transitional flow due to the complexity of the equation [16].

2.2.5 Other Affecting Factors

While heat transfer is most commonly affected by boundary conditions (i.e. pipe shape, heat conditions, etc.) material properties, and flow regime, there are other factors that contribute [20]. The most relevant of these factors are pipe roughness and entry length. All of the correlations and analytically derived Nusselt numbers assume smooth tubes. However, pipe roughness can drastically alter heat transfer characteristics. This occurs due to the roughness

of the pipe creating extra friction/turbulence at the wall [16]. In extreme cases (i.e. very high Re and roughness) the pipe roughness can extend into the viscous sublayer. The other major factor is the entry length. Before flow is fully developed, heat transfer is increased due to the reduction in boundary layer size [26]. This reduction in boundary layer size creates increased shear stress at the wall leading to higher friction and heat transfer values [26]. This effect is generally neglected as the entry length is generally orders of magnitude smaller than the entirety of the flow. However, in certain scenarios (such as heat sinks arrays or shorter piping systems) the entry length can have a significant impact on total heat transfer.

2.3. Natural Convection

This section discusses phenomena important to natural convection including the transition criteria and chimney effect. A variety of relevant Nusselt number correlations are also presented. Lastly, dependence on diameter, length, and Prandtl number are discussed. It is important to note that no constant heat flux internal natural circulation heat transfer correlation could be found by the author.

2.3.1 Natural Convection Phenomena

Similar to forced convection, natural convection transitions from laminar to turbulent flow. In 2010, Gyong-Uk Kang and Bum-Jin Chung performed a study to determine transition criteria in vertical pipes with high Prandtl numbers ($2000 < Pr < 3500$) [27]. High Prandtl numbers were used to allow the Grashof and Rayleigh numbers to be distinguishable. This was done as

previous literature disagreed on whether the transition to turbulent occurred at $10^9 = Ra_H$ [20] or $10^9 = Gr_H$ [28]. Kang and Chung used an analogous mass transfer system to reduce experimental uncertainties associated with difficulties in heat transfer systems. Measurements were taken for Grashof numbers between $Gr_H = 5.2 * 10^6 and\ 3 * 10^{10}$ to ensure laminar, transitional and turbulent flow were all captured. This experiment showed that transition to turbulent flow in vertical pipes occurs at roughly $Gr_H = 10^9$ with departure from the laminar region occurring at approximately $2.5 * 10^8 = Gr_H$ [27].

Another phenomenon of interest in natural convection is the chimney effect allows a higher flow rate to be induced through an open-ended adiabatic surface. This was first shown by Haaland and Sparrow and later improved on by various other researchers [29,30]. This technique is commonly employed in natural convection driven flows to improve heat transfer [30]. This enhancement depends primarily on the expansion ratio from channel to chimney with minimal dependence on the respective lengths of channel and chimney. These dependencies are complex and geometry dependent leading to optimal configurations for minimum maximum wall temperature and maximum heat transfer requiring different ratios of channel and chimney length and aspect ratios [30].

2.3.3 Natural Convection Correlations

A variety of heat transfer correlations/equations have been developed for cases involving natural convection. The most widely used of these are the Ostrach equation, the KATO

correlation and the Churchill correlation. The Ostrach equation is the only analytically derived method of determining heat transfer coefficients in natural circulation [31]. Similar to the Blasius solution, the Ostrach equation applies a similarity solution to convert Navier-Stokes into a system of ODEs yielding the following correlation [32]:

$$Nu_x = f_3(\mathrm{Pr}) * Gr_x^{0.25} \tag{21}$$

Where

$$f_3(\mathrm{Pr}) = \frac{0.53\sqrt{Pr}}{\left(0.61+1.22\sqrt{Pr}+1.24Pr\right)^{0.25}} \tag{22}$$

This correlation is valid for any Prandtl number and laminar flow ($Gr < 10^9$).

The most widely used empirically derived correlation for natural convection is the Churchill-Chu correlation for vertical isothermal surfaces.

$$Nu_L = \left(0.825 + \frac{0.387Ra_x^{\frac{1}{6}}}{\left(1+\left(\frac{0.492}{Pr}\right)^{\frac{9}{16}}\right)^{\frac{8}{27}}} \right)^2 \tag{23}$$

This correlation was proposed in 1975 and is valid for all flow regimes and Prandtl numbers [32]. While this equation was developed for external flow on vertical surfaces, it is widely used for vertical pipes [27]. The proposed reason for this is that prior to the boundary layers merging in internal flow, it can be accurately characterized as external flow. This occurs anytime $\delta(x) < D/2$ where $\delta(x)$ is the boundary layer thickness. Simplified versions of

Churchill-Chu were developed by Le Fevre (24) and Fouad (25) and can be used under more restrained circumstances [33,34].

$$Nu_L = 0.67Ra_H^{1/4} \tag{24}$$

For $Pr > 0.6\ and\ 10^4 < Ra < 10^9$

$$Nu_L = 0.31Ra_H^{0.28} \tag{25}$$

For $Pr > 0.6\ and\ 10^9 < Ra < 10^{13}$

Kang and Chung then tested these correlations using analogous mass transfer and modified them to [27]

$$Nu_L = 0.65Ra_H^{1/4} \tag{26}$$

For $Pr > 0.6\ and\ 10^4 < Ra < 10^9$

$$Nu_L = 0.11Ra_H^{0.28}Pr^{0.13} \tag{27}$$

For $Pr > 0.6\ and\ 10^9 < Ra < 10^{13}$

These equations matched experimental data for a range of high Prandtl number flows with error of less than 15%.

Many other correlations exist for varying geometries but the most applicable for the purposes of this thesis is developed for vertical ducts/chimneys [31]

$$Nu_R = \left[\left(\frac{\overline{Ra}}{C}\right)^m + \left(0.8\overline{Ra}^{\frac{1}{4}}\right)^m\right]^{\frac{1}{m}} \quad (28)$$

Where

$$\overline{Ra} = \frac{g\beta(T-T_\infty)R^4}{\nu\alpha L} < 10^5 \quad (29)$$

And for a circular duct. C= 16 and m=1. Substituting these values into equation 28 yields

$$Nu_R = \left(\frac{\overline{Ra}}{16}\right) + \left(0.8\overline{Ra}^{\frac{1}{4}}\right) \quad (30)$$

It should be noted that no source or method of derivation is mentioned for the origin of this correlation presented by Martinez.

2.3.4 Effects of Length, Diameter, and Prandtl Number

Many of the correlations presented in the previous section were derived using data from studies using low Prandtl number fluids with a limited range of lengths and geometries [35]. As such Ohk and Chung [36] and Kang and Yook [35] performed computational simulations validated with test sections to evaluate the effects of diameter, length, and Prandtl number. Ohk and Chung varied all three parameters computationally and compared the results with equations 27 and 28. Their simulation used unspecified pressure inlets and outlets with an isothermal wall. The results of these simulations confirmed the previously held belief that vertical pipe flow can be treated as external flow over a flat plate for heat transfer purposes when the boundary layers do not connect. This occurs at high Prandtl numbers and/or large

diameters. However, with lower Prandtl numbers and diameters, the Nusselt number was far lower than that predicted for flow over a flat plate. Ohk and Chung proposed a new correlation to accurately predict heat transfer in vertical pipes (equation 31).

$$Nu_L = 0.39 Gr_H^{0.52} Pr^{0.7} \left(\frac{H}{D}\right)^{-1.5} \quad (31)$$

This correlation is proposed to be valid when, $3.3 * 10^8 < Gr_L < 4.2 * 10^{11}, 0.7 < Pr < 20, and\ 20 < \frac{L}{D} < 300.$

In 2019, Kang and Yook published a similar study using an analogous mass transfer system and computational simulations to more accurately determine the effects of diameter and length with high Prandtl number [35].Similar to Ohk and Chung, pressure was used for both the inlets and outlets (specified at 0 Pa) and an isothermal wall was used for the final boundary condition. This study again verified that until the boundary layers interact, internal natural convection can be accurately described using external flat plate correlations. For pipes with very small diameters (d < 0.009m) heat transfer was impaired by up to 30% when compared to flat plate geometry. For slightly larger pipes (0.009m < d < 0.015m) heat transfer was over predicted by up to 15%. In pipes larger than 0.017m, external flow correlations were accurate within 3%.

These simulations also showed that previously suggested equations for boundary layer thickness (equation 32) were inaccurate and drastically under-predicted boundary layer thickness.

$$\delta = HRa_H^{-1/4} Pr^{\frac{1}{2}}, \delta_T = \delta Pr^{-1/2} \quad (32)$$

An alternative equation for boundary layer thickness was not presented. Interaction of boundary layers based upon entry length equations also showed an underprediction of entry length.

3. TOOLS AND METHODS

This section describes the tools and methods used in this study. All simulations were run using FLUENT 19.2. The general geometry and meshing is discussed first followed by relevant physical equations. Initial and boundary conditions are detailed next. The section concludes with descriptions of all simulated cases.

3.1 Tools

As discussed in the project motivation, only a computational model was used in this study. FLUENT v19.2 was the model of choice. FLUENT is a computational fluid dynamics software. FLUENT allows for easy tracking of all previously discussed quantities of interest (temperature, velocity, flow profiles, etc.) without any “disturbances” to the flow. FLUENT also tracks the effects of turbulence and conservation of energy.

3.2 Methods

This section details the computational setup/preprocessing methods for this study. This includes, simulated geometry, meshing, physical models, and initial and boundary conditions. It also includes a description of each case and the solver settings used for each simulation.

3.2.1. Geometry and Meshing

Only the heated portion of a simple natural circulation loop was modelled. The remainder of the loop was replaced using differential pressure boundary conditions to simulate the head produced from the loop drive. A more detailed description of this boundary condition can be found in section 3.3. The simulated geometry consists of a vertical pipe with radius 2.5 [cm]. The pipe consists of a 1 [m] heated portion at the inlet followed by an adiabatic section of varying length. Applying the 2-D axisymmetric assumption allows the geometry to be simplified to a rectangle with height equal to the radius and length equal to the height of the vertical pipe. Figure 5 shows the end of the heated geometry with imposed mesh. The bias of the mesh can be seen as the picture becomes black near the top and bottom borders.

A hard-biased quadrilateral mesh was used in all simulations. The mesh is biased towards the wall and centerline with a bias factor of 4. The number of vertical divisions was set to ensure a first cell height of approximately 1 for use with the $k-\omega$ model. Equally spaced cells were used horizontally with 500 divisions in the heated section. This number was determined based

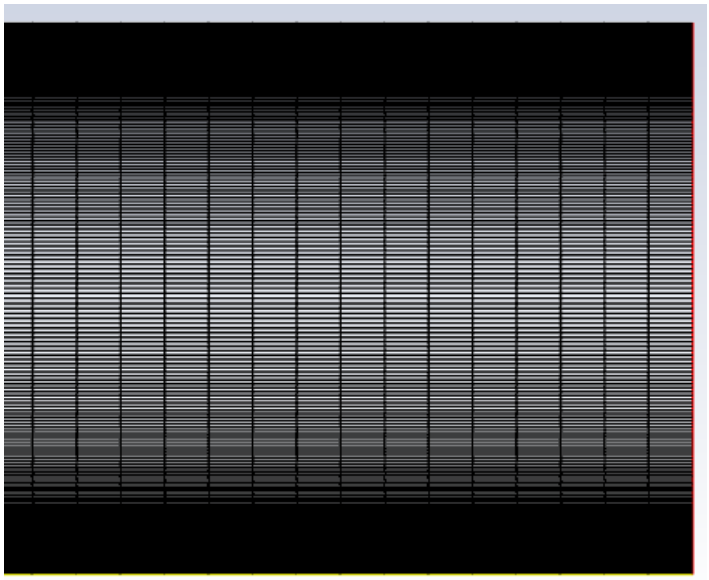

Figure 5: End of heated geometry with grid shown

off a GCI study discussed in section 4. The adiabatic had the same vertical spacing as the heated section but a less refined horizontal grid. This was done to decrease simulation time as all values of interest were taken in the heated section.

3.2.2. Physics Models

A 2-D axisymmetric model was applied for this problem to reduce computational requirements. This model simplifies flow from a three coordinate (x, y, z) system to a 2 coordinate (r, z) system by assuming flow is symmetric about the axis (figure 6). This is a reasonable assumption as the pipe is symmetric about its central axis and is symmetrically heated, therefore flow through the pipe should be axisymmetric. In a similar case, the 2-D

axisymmetric assumption was compared with a 3-d simulation and shown to reduce computational time by roughly 80% with a change in accuracy of approximately 1% [37].

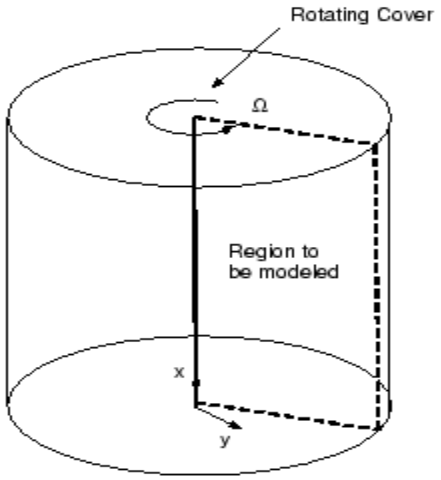

Figure 6: Model of axisymmetric modelling

The Navier Stokes equations are used to track transport of mass momentum and energy throughout the domain. These equations are simplified/modified due to the axisymmetric assumption as well as the chosen turbulence model and other approximations/assumptions. Simplified versions of all equations without the effects of turbulence are listed below.

Continuity:

$$\frac{1}{r}\frac{\partial(rv_r)}{\partial r} + \frac{\partial(v_z)}{\partial z} = 0 \tag{33}$$

r-momentum:

$$\rho\left(v_r\frac{\partial v_r}{\partial r}+v_z\frac{\partial v_z}{\partial z}\right)=-\frac{\partial \rho}{\partial r}+\mu\left(\frac{\partial^2 v_r}{\partial r^2}+\frac{1}{r}\frac{\partial v_r}{\partial r}-\frac{v_r}{r^2}+\frac{\partial^2 v_r}{\partial z^2}\right) \quad (34)$$

Z-momentum:

$$\rho\left(v_r\frac{\partial v_z}{\partial r}+v_z\frac{\partial v_z}{\partial z}\right)=-\frac{\partial \rho}{\partial z}+\mu\left(\frac{\partial^2 v_z}{\partial r^2}+\frac{1}{r}\frac{\partial v_z}{\partial r}+\frac{\partial^2 v_z}{\partial z^2}\right)-\rho g_z\beta\Delta T \quad (35)$$

Energy:

$$\rho c_p\left(\frac{v_r\partial T}{\partial r}+\frac{v_z\partial T}{\partial z}\right)=k\left(\frac{1}{r}\frac{\partial}{\partial r}\left(r\frac{\partial T}{\partial r}\right)+\frac{\partial^2 T}{\partial z^2}\right) \quad (36)$$

It is important to note that the effects of natural convection are incorporated into the z-momentum equation by the addition of the $\rho g_z\beta\Delta T$ term. This approximation, known as the Boussinesq approximation, assumes that only the density of the fluid changes with changing temperature and that this change in density only needs to be accounted for when multiplied by gravity [38].

The k-ω SST model is used for all simulations in this study. This model was chosen due to its explicit treatment of flow near the wall and accuracy in the free stream. The k-ω SST model is identical to the k-ω model except that the k-ω SST model combines the k-ϵ and k-ω models with a blending function [39]. This blending function causes the k-ω model to dominate near the wall and the k-ϵ model to dominate in the free stream while blending the two results in-between. There are other minor differences between the k-ω and k-ω SST models that are not discussed as they are outside the scope of this thesis.

In this turbulence model the main quantities of interest are k, the turbulent kinetic energy, and ω, the specific dissipation rate. A physical interpretation of the turbulent kinetic energy is the energy in the flow that is contained within the eddies. The specific dissipation rate is the rate that k (turbulent kinetic energy) is turned into thermal internal energy or the mean frequency of turbulence. Specific dissipation can also be defined as turbulent dissipation over turbulent kinetic energy ($\frac{\epsilon}{k}$).

3.2.3. Initial and Boundary Conditions

Initial conditions for all simulations are detailed in Table 1 below. Water is used as the fluid for all simulations. For all 10 [kW] simulations, water properties were used based on water at atmospheric pressure at 300K. To ensure boiling temperatures are not reached, simulations with higher heat flux use water properties of water at 300K at 150 [bar] (approximate PWR pressure).

Table 1: Initial conditions for all simulations

Fluid	Water
Temperature	300K
Axial Velocity	0.2 [m/s]
Radial Velocity	0
Turbulent Kinetic Energy	1e-05 [m^2/s^2]
Specific Dissipation Rate	1 [1/s]
Gauge Pressure	0 [Pa]

Boundary conditions for all simulations are detailed in Table 2. The bottom boundary is an axis boundary condition and acts as the axis of revolution or centerline for the pipe. The left and right boundaries are a pressure inlet and outlet respectively. Backflow conditions for turbulent kinetic energy and specific dissipation rate are identical to initial conditions. Inlet pressure is varied with pipe height based on the process described in section 3.4. Outlet pressure is set at a constant value of 0 [Pa]. The upper boundary is a no-slip wall with constant heat flux varied by case ranging from 10 to 500 [kW/m^2]. All other initial and boundary conditions are set as fluent defaults.

Table 2: Boundary conditions for all simulations

Boundary Location	**Boundary Type**
Bottom Boundary	Axis
Left Boundary	Pressure Inlet (pressure varies by case)
Right Boundary	Pressure Outlet (0 Pa)
Top Boundary	Wall with Constant Heat Flux (flux varies by case)or adiabatic

3.2.4. Case Descriptions

Cases for this thesis involve varying the wall heat flux and inlet pressure. Inlet pressure varies with height of the simulated section. Determining the case pressure requires a 5-step iterative process detailed below:

1. Run a simulation with an initial guess for inlet pressure.
2. Determine the average temperature of the fluid in the simulated section (hot leg) of pipe.

3. Use this average temperature to calculate the difference in density between the hot and cold leg of the pipe.
4. Convert the density difference into a pressure difference.
5. Repeat process with calculated pressure difference as initial guess until pressure change is on the order of 10^{-1} Pa.

Heat flux is increased beginning at 10 [kW/m^2] and ending at 500 [kW/m^2]. It is important to recall that fluid properties must be varied for higher heat flux to avoid temperatures consistent with saturation and boiling. Table 3 details height and wall heat flux for all simulated cases.

Table 3: Matrix of simulations performed

Heat Flux [kW/m^2] / Height [m]	10	100	250	500
1	X	X	X	X
2	X	X	X	X
5	X	X	X	X
10	X	X	X	X

3.2.5. Solver Settings

This section details all relaxation factors and iterative methods used. Table 4 details the numerical schemes used for simulations. It is important to note that convergence was only achieved for all cases using the FLUENT coupled solver for pressure-velocity coupling. Other widely used methods such as SIMPLE, SIMPLEC, and PISO had difficulties converging with fine

grid sizes or low-pressure gradients. Table 5 details the relaxation factors used in all simulations. Convergence was only obtained by raising the momentum relaxation factor and slightly lowering the relaxation of turbulent factors.

Table 4: Solution methods for all simulations

Quantity of interest	Method
Pressure-Velocity Coupling	Coupled
Gradient	Least-squares
Pressure	Linear
Momentum	Second Order Upwind
Turbulent kinetic energy	QUICK
Specific Dissipation	QUICK
Energy	QUICK

Table 5: Relaxation factors for all simulations

Quantity of interest	Relaxation Factor
Pressure	0.3
Momentum	0.8
Density	1
Body Forces	1
Turbulent Kinetic Energy	0.75
Specific Dissipation Rate	0.75
Turbulent Viscosity	1
Energy	0.75

4. FLUENT VERIFICATION

Verification for this thesis is approached from three directions. The first of these is monitoring of residuals. Iterations for all simulations were continued until residuals were below 1 E-3 for

mass, 1 E-5 for turbulence and velocity parameters, and 1 E-6 for Energy. After ensuring residuals are sufficiently small, quantities of interest are monitored. For the purposes of this study these quantities are velocity and temperature. These quantities are the most important as the directly correlate to HTC and friction factor. The final step in verification is performing a grid convergence index (GCI) study in accordance with ASME V&V 20.2009.

The goal of performing a GCI is to ensure that numerical results are independent of the physical accuracy [40]. Because all simulations were steady state, only a spatial grid convergence index was performed. To ensure spatial independence, a minimum of three different grids with an average cell size ratio of at least 1.3 must be analyzed. This cell size ensures sufficient differences in the grid for spatial independence. The cell ratio for this GCI study was 1.5874. Quantities of interest from each of the three grids are then analyzed and used to determine the GCI and uncertainty. For this thesis the computational heat transfer coefficient was chosen as the quantity of interest as determining its accuracy/validity is the primary goal.

These values lead to an apparent order of 6.25 for the solution methods. The extrapolated relative error is 0.0011% leading to an adjusted GCI of .0147. This GCI can be used to calculate an interval of 95% confidence of $\pm 0.0128\%$. Figure 7 shows the calculated HTC values for each of the three grids analyzed along with an exponential trendline to demonstrate the convergence of the grid.

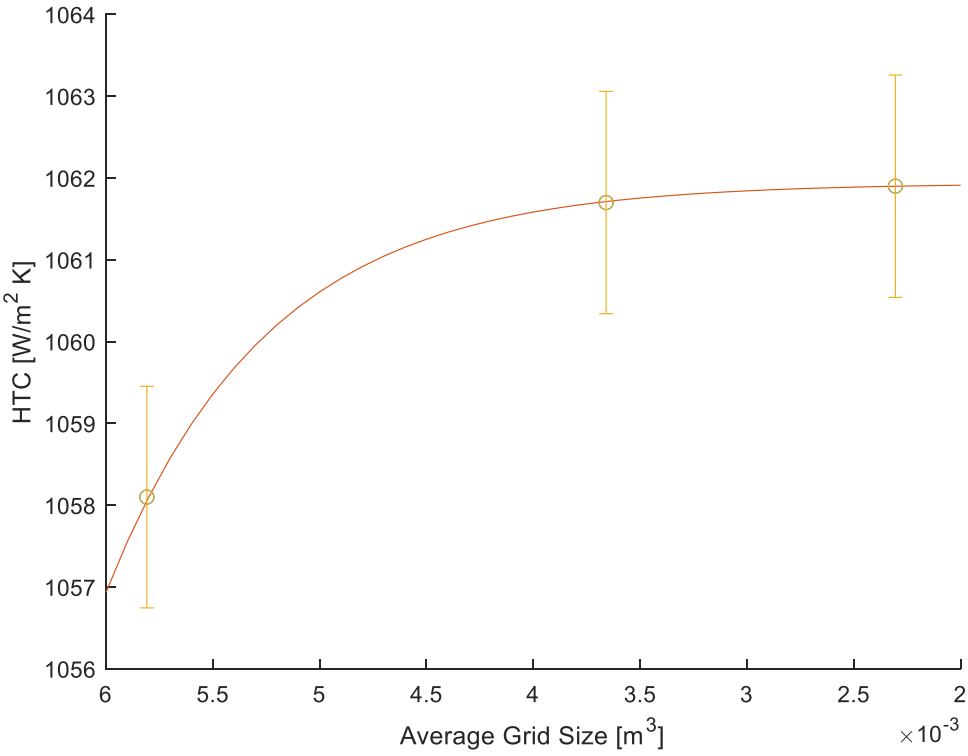

Figure 7: Computed HTCs with uncertainty for varying grid sizes

5. FLUENT RESULTS AND ANALYSIS

This section contains all results for this thesis. This includes relevant temperature and velocity profiles, comparison of heat transfer coefficients, and comparison of friction factors. Heat transfer coefficients are compared with values obtained from the Gnielinski correlation based on heat flux and height. Friction factors are compared with both laminar and turbulent friction factor correlations. Cases are described as QXX.YY where XX is the constant heat flux in KW and YY is the simulated height in meters, e.g. Q500.5 signifies a constant heat flux of 500 KW and a height of 5m.

5.1. Temperature and Velocity Profiles

As discussed previously, heat transfer and friction factor can be directly determined from temperature and velocity profiles. As such, velocity and temperature profiles were saved for every simulation (Appendix A). Temperature and velocity profiles at various locations throughout the heated section are shown in figures 8a-d. For all simulations without a chimney, profiles were taken at 0.25, 0.5, 0.75 and 1m from the pipe entry to show the development of the thermal and momentum boundary layers. It is important to note that neither boundary layer reaches a fully developed state by the exit of the heated section (20 diameters from entrance). This is important as most correlations neglect entry length effects in pipes longer than 5-10 diameters [31]. For simulations with a chimney, temperature and

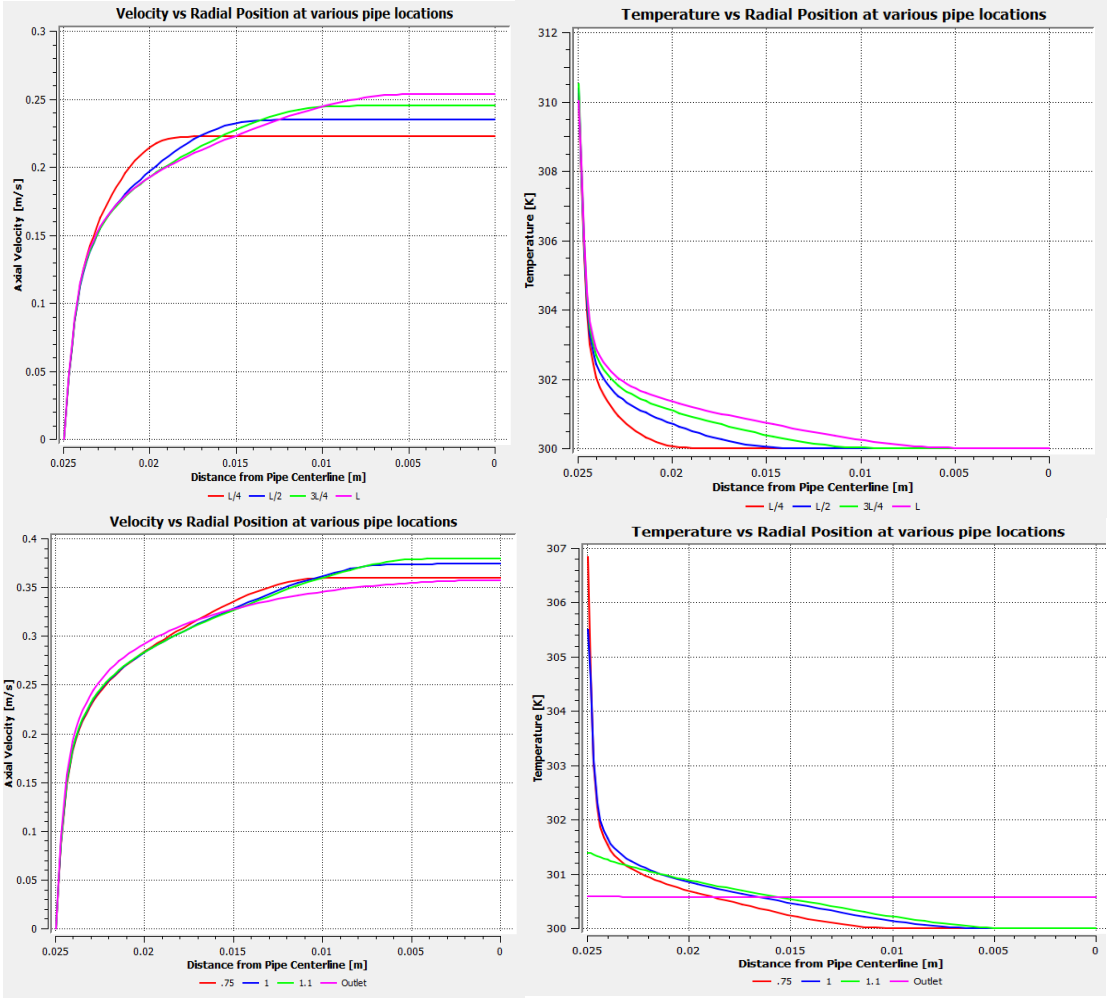

Figure 8a-d: Representative temperature and velocity profiles. 8a and 8b show geometry without a chimney while 8c and 8d show profiles with a chimney.

velocity profiles were taken at 0.75, 1, 1.1m and chimney outlet. These profiles demonstrate the rate the flow reverts to shapes expected of forced flow conditions. Both temperature and velocity profiles reach shapes consistent with forced flow by the outlet of the 5m section.

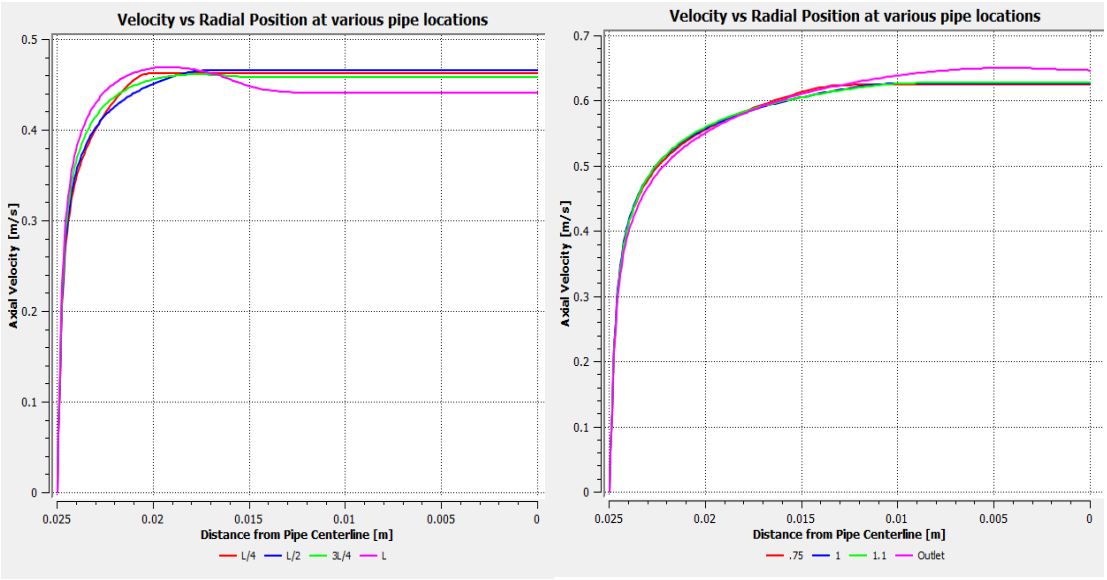

Figure 9a&b: Velocity profiles for cases Q500.1 and Q500.2

The “wall peak” expected from natural convection was only clearly visible in the 500.1 case and slightly visible in the 500.2 case (figure 9a&b). The existence of the wall peak is important as it validates that the computational model can capture the wall peak. The wall peak most likely does not appear in other simulations as it is washed out by the turbulence in the flow. Contour plots of temperature and velocity for bounding cases are pictured in figures 10-12. These contours demonstrate the rate at which boundary layers develop throughout the heated section. It is interesting to note that as the heat flux increases, the velocity profile develops much more quickly while the temperature profile develops more slowly. This relation is most likely due to the increase in driving head/turbulence. The temperature contours also display the drastic slowing of temperature profile development with increased heat flux.

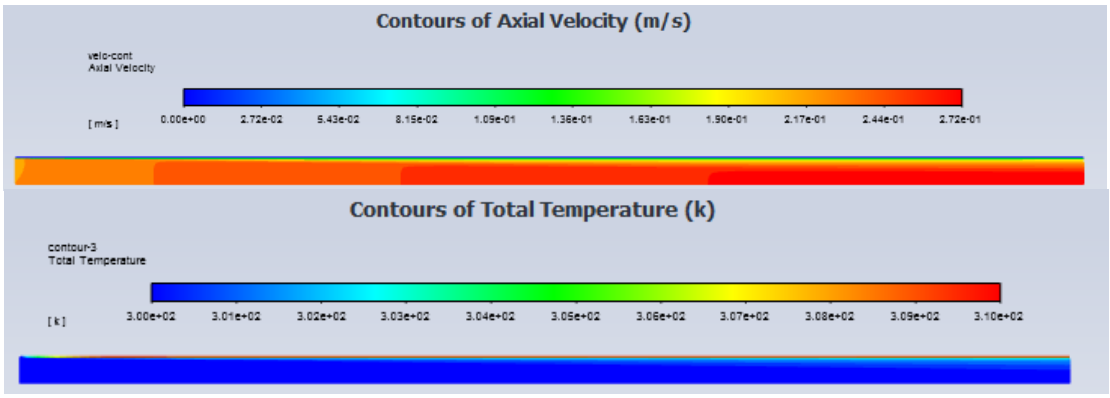

Figure 10: Q10.1 temperature and velocity contours

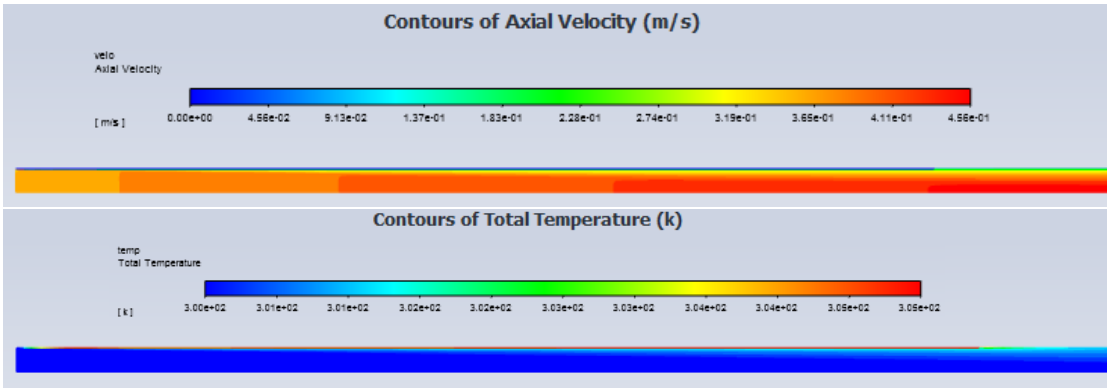

Figure 11: Q10.10 heated section temperature and velocity contours

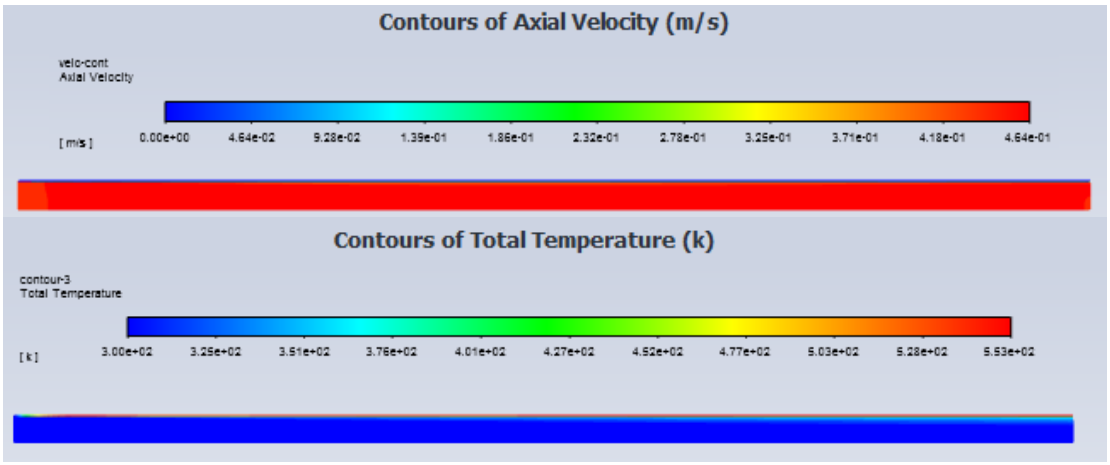

Figure 102: Q500.1 temperature and velocity contours

5.2. Heat Transfer Coefficients

Averaged Heat transfer coefficients were calculated for all cases and compared to laminar, turbulent, and a variety of natural convection Nusselt number correlations (Ohk Chung, flat plate, chimney, etc.). It is important to note that all Nusselt number correlations found were developed for constant temperature, not constant heat flux. Local HTCs were calculated throughout the grid using equation 37.

$$HTC_{Local} = \frac{Q}{dT} = \frac{Q}{T_{wall} - T_{centerline}} \quad [37]$$

Table 6: Comparison of average HTCs and the Gnielinski correlation

Case	Gnielinski HTC $\left[\frac{W}{m^2K}\right]$	Computational HTC $\left[\frac{W}{m^2K}\right]$	Percent difference [%]
10.1	1245.8	1215.4	2.50
10.2	1511.1	1349.9	11.95
10.5	1755.3	1921.1	-8.63
10.10	1882.1	2331.3	-19.27
100.1	2468.6	2067.1	19.42
100.2	3041.6	2013.3	51.07
100.5	3545.8	2400.5	47.71
100.10	3796.8	2589.7	46.61
250.1	2842.6	2429.5	17.00
250.2	3547.8	2411.6	47.11
250.5	4161.7	2889.4	44.04
250.10	4455.6	3123.5	42.65
500.1	3242.6	2836.2	14.33
500.2	4108.7	2864.8	43.42
500.5	4832.4	3454.5	39.89
500.10	5173.9	3746.3	38.11

Where Q is the constant heat flux and T_x is the temperature at the wall or centerline. All local HTCs were then averaged to determine the average HTC. The average HTC was then compared with a variety of existing correlations. The Gnielinski correlation was used for turbulent flow and was the only correlation in the same order of magnitude as HTCs calculated from simulation results. Table 6 compares the averaged HTC and the Gnielinski HTC.

The calculated Gnielinski correlation was used with the previously calculated dT values to determine what the local heat flux would be using equation 38.

$$Q_{Gnielinski} = dT * HTC_{Gnielinski} \quad [38]$$

Figures 13&14 compare the calculated Gnielinski heat flux and simulated heat flux along the heated section of the pipe. All cases follow a similar trend along the length of the heated section of pipe. The heat flux increases steeply as flow enters the pipe and peaks around 2 diameters. This peak occurs when heat diffusion through the liquid overcomes heat diffusion into the liquid. The HTC then drops slightly and begins a slow rise until the end of the heated section. This drop occurs as advective terms begin to overcome diffusive terms. When a chimney is present, the HTC drops slightly before the end of the heated section due to the reduction in wall temperature in the chimney.

For all cases except the Q10.YY cases, the increase in height follows an extremely similar pattern. For the initial case (case without a chimney) the HTC is slightly over-predicted (~15%)

by the Gnielinski correlation. The HTC for all additional cases (those with a chimney) is then drastically overpredicted (40+%) by the Gnielinski correlation. As the chimney height increases, the overprediction decreases slightly. For the Q10.YY cases the initial case is nearly identical (<3% difference) to the Gnielinski HTC. A smaller increase in overprediction occurs with the addition of the chimney than in the higher heat flux cases. As the chimney height increases, the Gnielinski correlation underpredicts the HTC.

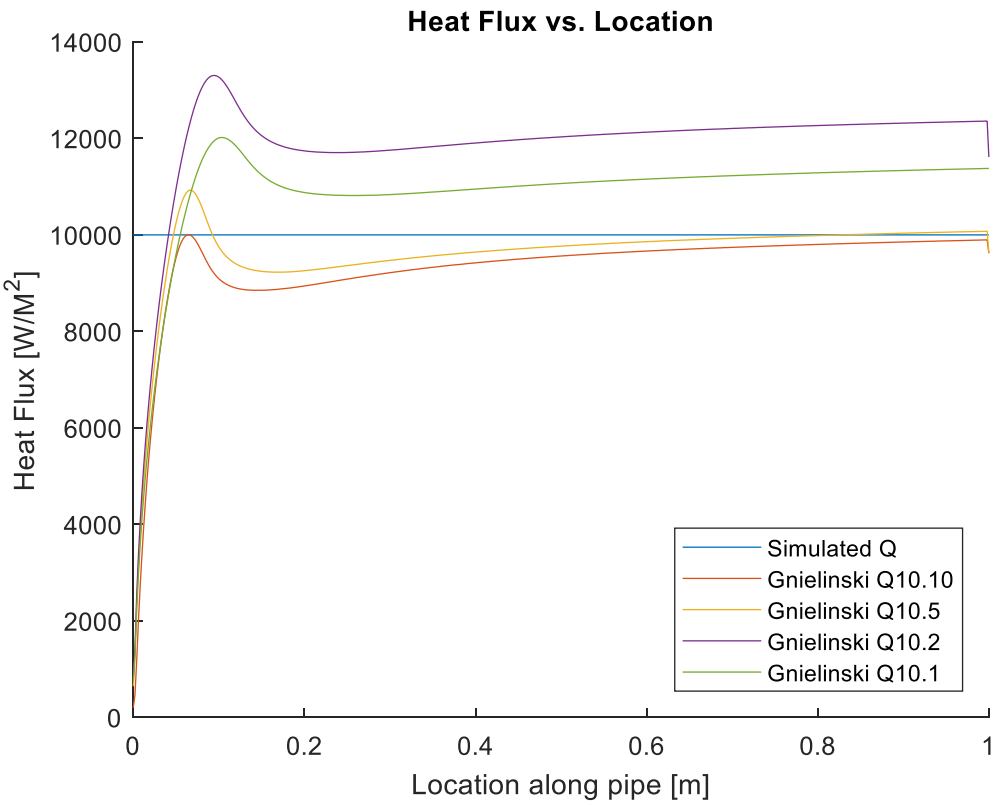

Figure 12: Heat flux along pipe for q=10,000 [W/m^2]

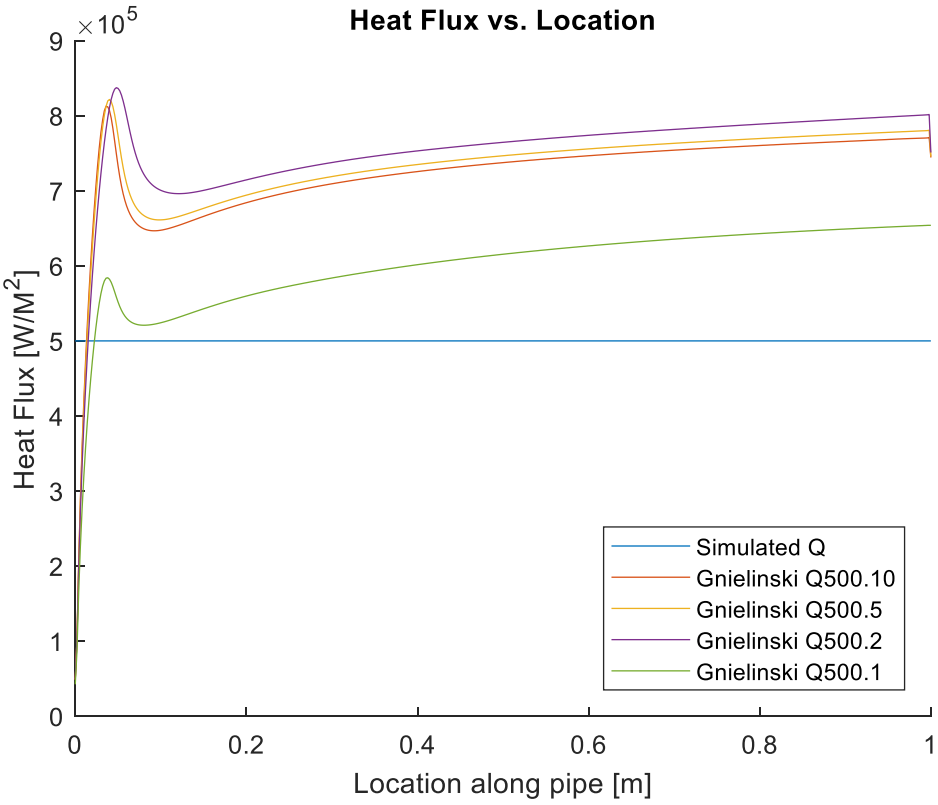

Figure 13: Heat flux along pipe for q=500,000 [W/m^2

Figures 15&16 compare the averaged HTC and the Gnielinski HTC by height and heat flux. The straight line on each of these graphs represents a perfect approximation by the correlation. It is interesting to note that the "slope" of cases with a chimney and identical heat flux remain virtually constant except for the Q10.YY cases. The cases without a chimney further show the lowest heat flux cases as outliers as the slope of the L=1m changes after the first data point. The reason for these differences is unclear but could occur due to the minimal temperature

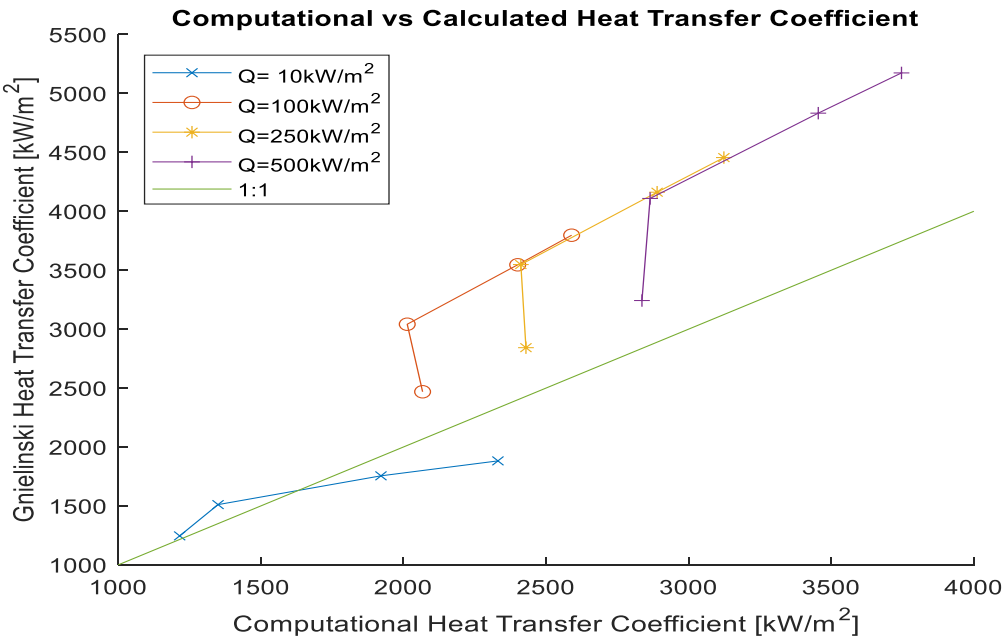

Figure 14: Comparison of Calculated and Simulated HTC with specified heat flux

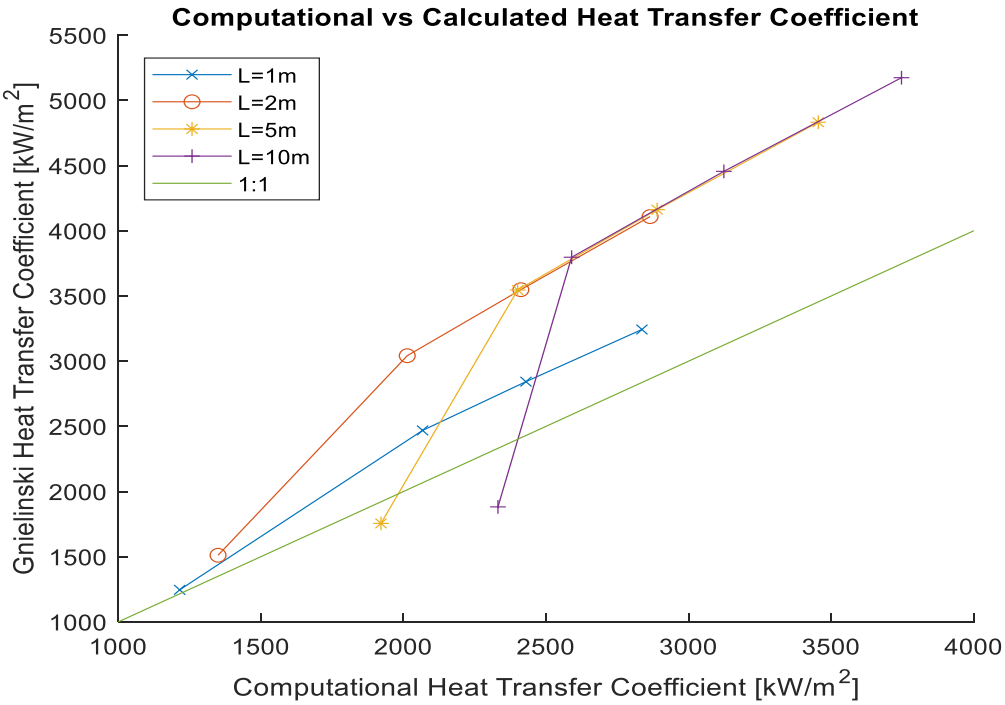

Figure 15: Comparison of Calculated and Simulated HTC with specified length

differential between the wall and fluid centerline. This minimal difference could cause the natural circulation effects to be more easily washed out by the pressure differential. The difference may also indicate that the relation between the Gnielinski correlation and natural circulation HTC is non-linear.

All previous charts were generated using the centerline temperature as the bulk temperature as is common for external flow. For internal flow, the average temperature is generally used due to the complexity of measuring internal centerline temperature without disrupting the flow [23,24]. As such figures 15 and 16 were recreated using average temperature in place of centerline temperature. Figures 17&18 show these results. Many trends between the two graphs remained similar. However, cases without a chimney were increasingly overpredicted as heat flux increased. As heat flux increased, the "jump" caused by the addition of a chimney also lessened. Both of these differences most likely occur due to the increase in turbulence from the higher heat fluxes. This increase pulls heat away from the wall raising the average temperature faster as heat flux increases. This is exceptionally well demonstrated by the Q500 cases as they show no significant change in slope regardless of chimney height.

To quantify the maximum discrepancy of results due to viscosity being held constant, the case with the highest temperature differential (Q500.1) was run with changing viscosity. The viscosity change was modelled as a linear function between 300 and 500K and predicted an HTC of approximately 10% lower than the Q500.1 case without changing viscosity.

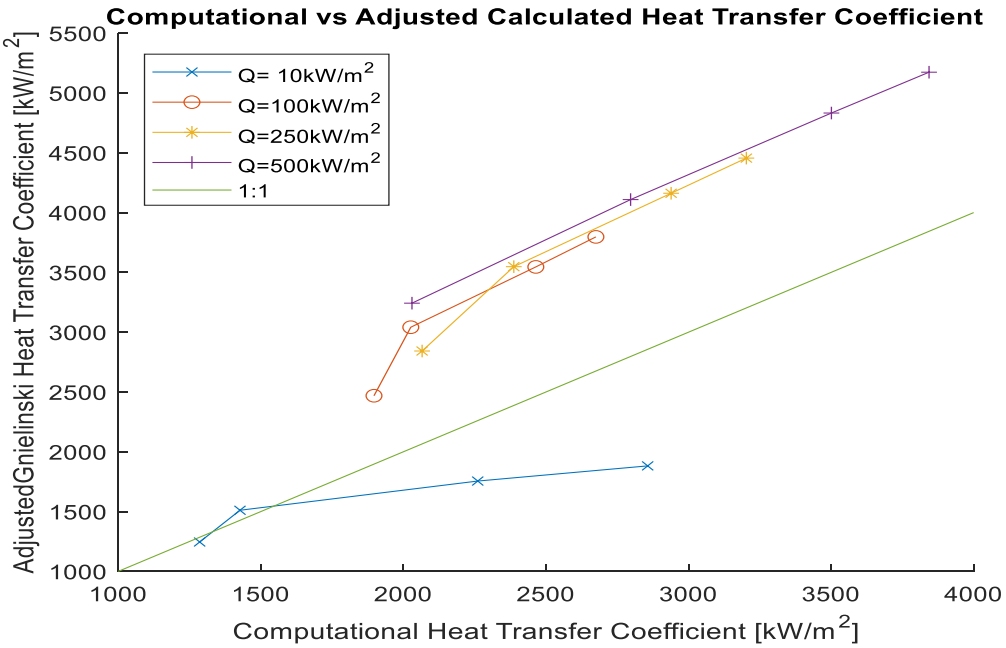

Figure 16:Comparison of Calculated and Simulated HTC using Tav with specified flux

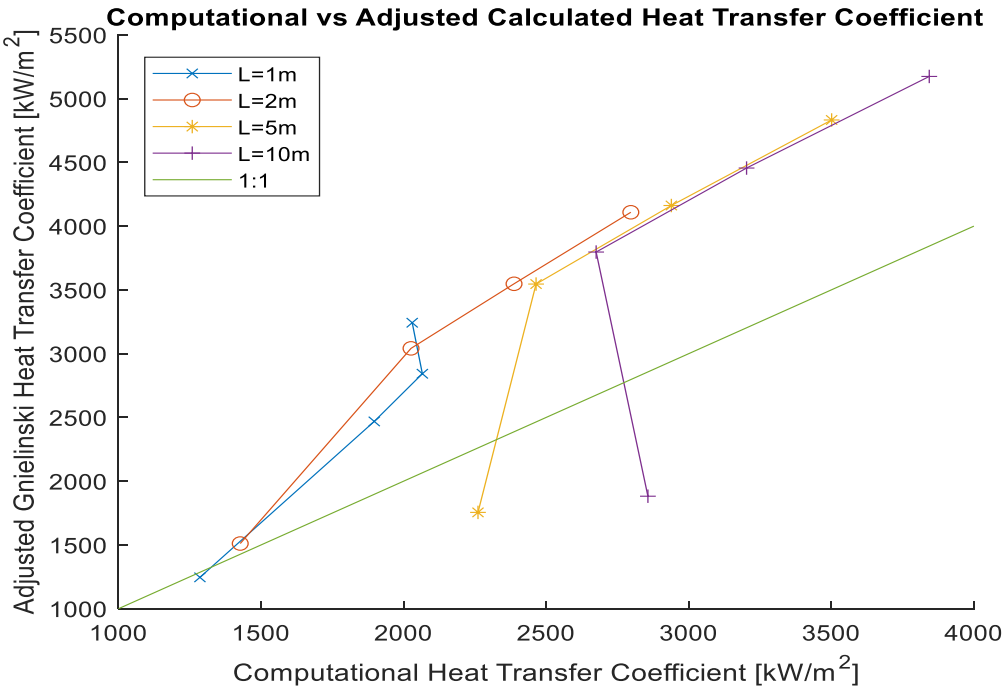

Figure 17: Comparison of Calculated and Simulated HTC using Tav with specified flux

5.3 Friction Factor

The friction factor for each case was calculated using equation 16. The velocity 0.0001 m from the wall was used to approximate the $\frac{du}{dy}|_{wall}$ term in equation 16. Figure 19 compares these calculated friction factors with laminar and turbulent friction factors calculated using Re_D numbers calculated using mean fluid velocity. The upper lines represent friction factors calculated using classical turbulent correlations and the lower lines represent those calculated using laminar correlations. Calculated friction factors are represented by data points located

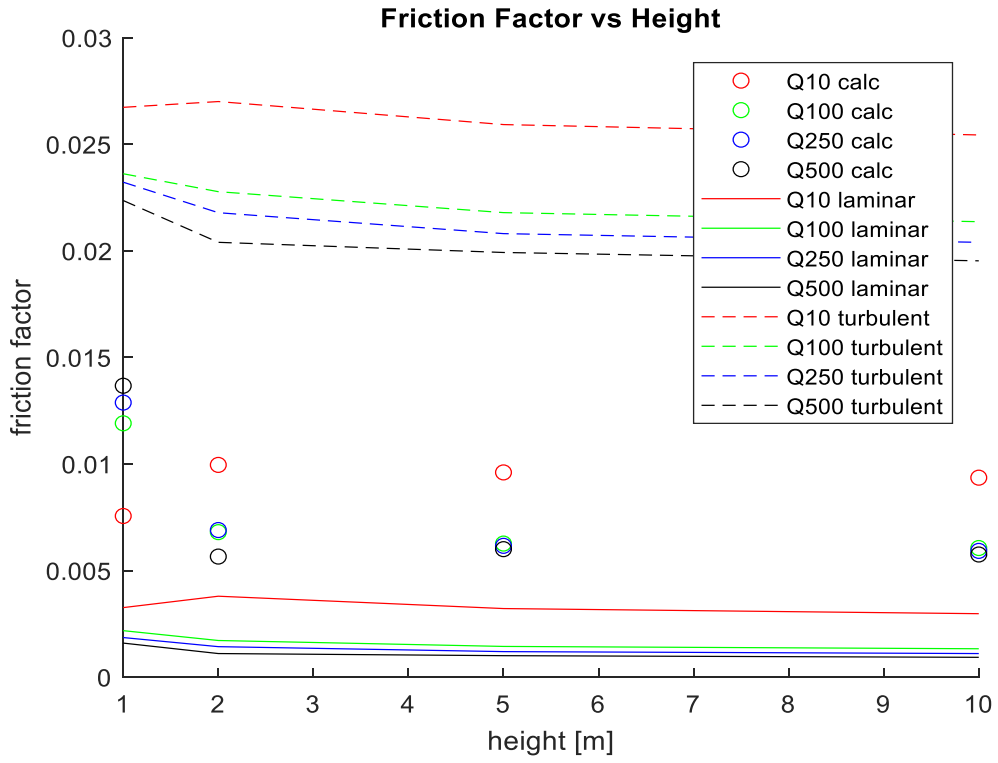

Figure 18: Comparison of calculated friction factor with laminar and turbulent correlations vs height.

between the lines. The color can be used to compare the calculated value of a particular case with the laminar and turbulent values.

All calculated values fall between the laminar and turbulent values. This is expected as the natural circulation profile has a steeper slope at the wall than a laminar profile but a less steep slope than turbulent profiles. Similar to the heat transfer calculations, the friction factors follow a similar pattern for all cases except the Q10.YY cases. The Q10.YY cases have an increase in friction factor with the inclusion while all other heat fluxes drop by 50+% with the inclusion of the chimney. However, this does follow the pattern of existing correlations as both the laminar and turbulent friction factors increase from Q10.1 to Q10.2. All calculated friction factors for chimney cases are 60-70% lower than turbulent values while cases without a chimney (excluding Q10.1) are 40-50% lower.

The effects of holding viscosity constant on calculated friction factor were quantified similar to the HTC. For the maximum case, the friction factor calculated with varying viscosity was approximately 15% lower than the Q500.1 case with constant viscosity.

6. CONCLUSIONS AND FUTURE WORK

New nuclear power plant designs (such as NuScale's SMR) rely on natural circulation to circulate coolant. The codes used in the design of these reactors rely on laminar and turbulent heat transfer correlations and friction factors. However, in most cases, these correlations cannot accurately predict friction factor or HTC when iso-flux natural circulation is the driving

force. This error most likely occurs due to the difference in flow profile caused by the increased buoyancy of the heated fluid. Deviations in HTCs from existing turbulent correlations decreased with increasing heat flux and chimney height while deviations from friction factor remained relatively constant. The removal of an adiabatic chimney caused a significant reduction in error for HTCs but had no impact on friction factor. The minimally heated cases appeared to be outliers and did not follow trends present throughout all other cases. This is most likely due to heating of fluid near the wall being insufficient to generate a large buoyancy difference. Future physical and computational experiments must be carried out to develop an accurate correlation for prediction of iso-flux natural circulation heat transfer coefficients and friction factors.

7. REFERENCES

[1] WEISBACH, J. (1845). LEHRBUCH DER INGENIEUR- UND MASCHINEN-MECHANIK, VOL. 1. THEORETISCHE MECHANIK, VIEWEG UND SOHN, BRAUNSCHWEIG. 535 PAGES (IN GERMAN).

[2] D'AUBUISSON, J. F. (1834). TRAITÉ DE L'HYDRAULIQUE À L'USAGE DES INGÉNIEURS, PITOIS-LEVRAULT, PARIS (IN FRENCH).

[3] POISEUILLE, J. L. (1841). "RECHERCHES EXPÉRIMENTALES SUR LE MOUVEMENT DES LIQUIDES DANS LES TUBES DE TRÈS-PETITS DIAMÈTRES." COMPTES RENDUS, ACADÉMIE DES SCIENCES, PARIS 12, 112 (IN FRENCH).

[4] HAGEN, G. (1839). "ÜBER DIE BEWEGUNG DES WASSERS IN ENGEN ZYLINDRISCHEN RÖHREN."POGG. ANN., 46, 423-442 (IN GERMAN)

[5] ROUSE, H. AND INCE, S. (1957). HISTORY OF HYDRAULICS, IOWA INSTITUTE OF HYDRAULIC RESEARCH, UNIV. OF IOWA, IOWA CITY, 269 PG.

[6] DARCY, H. (1857). RECHERCHES EXPÉRIMENTALES RELATIVES AU MOUVEMENT DE L'EAU DANS LES TUYAUX, MALLET-BACHELIER, PARIS. 268 PAGES AND ATLAS (IN FRENCH).

[7] BROWN, GLENN. (2002). THE HISTORY OF THE DARCY-WEISBACH EQUATION FOR PIPE FLOW RESISTANCE. PROC. ENVIRON. WATER RESOUR. HIST. 38. 10.1061/40650(2003)4.

[8] FANNING, J. T. (1877). A PRACTICAL TREATISE ON WATER-SUPPLY ENGINEERING, VAN NOSTRAND, NEW YORK, 619 PAGES.

[9] REYNOLDS, O. (1883). "AN EXPERIMENTAL INVESTIGATION OF THE CIRCUMSTANCES WHICH DETERMINE WHETHER THE MOTION OF WATER SHALL BE DIRECT OR SINUOUS AND OF THE LAW OF RESISTANCE IN PARALLEL CHANNEL." PHIL. TRANS. OF THE ROYAL SOC., 174:935-982.

[10] BLASIUS, H. (1913). DAS ÄHNLICHKEITSGESETZ BEI REIBUNGSVORGÄNGEN IN FLÜSSIGKEITEN, FORSCHUNGS-ARBEIT DES INGENIEUR-WESENS 131. (IN GERMAN).

[11] KÁRMÁN, TH. VON (1930). "MECHANISCHE AEHNLICHKEIT UND TURBULENZ." PROC. THIRD INTERNATIONAL CONGRESS FOR APPLIED MECHANICS, C. W. OSEEN AND W. WEIBULL EDS., STOCKHOLM. VOL. 1, 79-93 (IN GERMAN).

[12] NIKURADSE, J. (1933). "STRÖMUNGSGESETZE IN RAUHEN ROHREN." FORSCHUNGS-ARBEIT DES INGENIEUR-WESENS 361 (IN GERMAN).

[13]BIRD, R. BYRON; STEWART, WARREN E.; LIGHTFOOT, EDWIN N. (2002). *TRANSPORT PHENOMENA* (2ND ED.). NEW YORK: J. WILEY. PP. 318, 359.

[14]CHAUDHRY, M. H. (2013). *APPLIED HYDRAULIC TRANSIENTS* (3RD ED.). SPRINGER. P. 45

[15]KANG, GYEONG-UK & CHUNG, BUM-JIN. (2010). THE EXPERIMENTAL STUDY ON TRANSITION CRITERIA OF NATURAL CONVECTION INSIDE A VERTICAL PIPE. INTERNATIONAL COMMUNICATIONS IN HEAT AND MASS TRANSFER - INT COMMUN HEAT MASS TRANS. 37. 1057-1063. 10.1016/J.ICHEATMASSTRANSFER.2010.06.016.

[16]*ÇENGEL, YUNUS; TURNER, ROBERT; CIMBALA, JOHN (2017). FUNDAMENTALS OF THERMAL-FLUID SCIENCES (FIFTH ED.). NEW YORK, NY.*

[17]GARBRECHT, OLIVER. (2017). LARGE EDDY SIMULATION OF THREE-DIMENSIONAL MIXED CONVECTION ON A VERTICAL PLATE. 10.18154/RWTH-2018-221554.

*[18]*GEANKOPLIS, C.J. *TRANSPORT PROCESSES AND SEPARATION PROCESS PRINCIPLES* (2003). THIRD EDITION, PP. 438-440.

*[19]*HEWITT, G. F., SHIRES, G. L., AND BOTT, T. R. (1994) *PROCESS HEAT TRANSFER*, MCGRAW-HILL

*[20]*Incropera, F. P. and DeWitt, D. P. (1990) *Fundamentals of Heat and Mass Transfer*, John Wiley and Sons.

*[21]*Satish G. Kandlikar,Chapter 3 - Single-Phase Liquid Flow in Minichannels and Microchannels,Editor(s): Satish G. Kandlikar, Srinivas Garimella, Dongqing Li, Stéphane Colin, Michael R. King,Heat Transfer and Fluid Flow in Minichannels and Microchannels (Second Edition),Butterworth-Heinemann,2014,PP. 103-174

*[22]*Kays, W. M., and Crawford, M. E. Convective Heat and Mass Transfer. 3rd ed. New York: McGraw-Hill, 1993. Print. McGraw-Hill Ser. in Mechanical Engineering.

*[23]*Dittus, Frederick William, and Boelter, L. M. K. Heat Transfer in Automobile Radiators of the Tubular Type. Berkeley, Calif: U of California, 1930. Print. University of California Publications in Engineering, v. 2, No. 13.

[24]SIEDER, E. N., AND G. E. TATE. "HEAT TRANSFER AND PRESSURE DROP OF LIQUIDS IN TUBES." *INDUSTRIAL & ENGINEERING CHEMISTRY* 28.12 (1936): 1429-435. WEB.

[25]GNIELINSKI, V. NEUE GLEICHUNGEN FÜR DEN WÄRME- UND DEN STOFFÜBERGANG IN TURBULENT DURCHSTRÖMTEN ROHREN UND KANÄLEN. *FORSCH ING-WES* 41, 8–16 (1975) DOI:10.1007/BF02559682

[26]HAYES, ROBERT E., ANDRÉS DONOSO-BRAVO, AND JOSEPH P. MMBAGA. "ENTRY LENGTH EFFECTS FOR MOMENTUM, HEAT AND MASS TRANSFER IN CIRCULAR

DUCTS WITH LAMINAR FLOW." *CANADIAN JOURNAL OF CHEMICAL ENGINEERING* 93.5 (2015): 863-69. WEB.

[27]KANG, GYEONG-UK & CHUNG, BUM-JIN. (2010). THE EXPERIMENTAL STUDY ON TRANSITION CRITERIA OF NATURAL CONVECTION INSIDE A VERTICAL PIPE. INTERNATIONAL COMMUNICATIONS IN HEAT AND MASS TRANSFER - INT COMMUN HEAT MASS TRANS. 37. 1057-1063. 10.1016/J.ICHEATMASSTRANSFER.2010.06.016.

[28]A. BEJAN, J.L. LARGE, THE PRANDTL NUMBER EFFECT ON THE TRANSITION IN NATURALCONVECTION ALONG A VERTICAL, JOURNAL OF HEAT TRANSFER 112 (1990) 789–790.

[29]S.E. HAALAND, E.M. SPARROW, SOLUTIONS FOR THE CHANNEL PLUME AND THE PARALLEL-WALLE DCHIMNEY, NUMER. HEATTRANSFER 6 ,1983) 155±172.

[30]AULETTA, A. & MANCA, ORONZIO & MORRONE, BIAGIO & NASO, VINCENZO. (2001). HEAT TRANSFER ENHANCEMENT BY THE CHIMNEY EFFECT IN A VERTICAL ISOFLUX CHANNEL. INTERNATIONAL JOURNAL OF HEAT AND MASS TRANSFER. 44. 4345-4357. 10.1016/S0017-9310(01)00064-3.

[31]MARTINEZ, ISODORO (2015), FORCED AND NATURAL CONVECTION. WEB

[32]OSTRACH, S. (1953). AN ANALYSIS OF LAMINAR FREE-CONVECTION FLOW AND HEAT TRANSFER ABOUT A FLAT PLATE PARALLEL TO THE DIRECTION OF THE GENERATING BODY FORCE.

[33]E.J. LE FEVRE, A.J. EDE, LAMINAR FREE CONVECTION FROM THE OUTER SURFACE OF A VERTICALCIRCULAR CYLINDER, PROCEEDINGS OF THE NINTH INTERNATIONAL CONGRESS APPLIEDMECHANICS, BRUSSELS, 1956, PP. 175–183

[34]M.G. FOUAD, N. IBL, NATURAL CONVECTION MASS TRANSFER AT VERTICAL ELECTRODES UNDERTURBULENTFLOW CONDITIONS, ELECTROCHIMICA ACTA 3 (1960) 233–243

[35]KANG GYEONG-UK, YOOK DAE-SIK, (2019) LAMINAR NATURAL CONVECTION HEAT TRANSFER DEPENDING ON DIAMETERS OF VERTICAL CYLINDERS WITH CIRCULAR CROSS-SECTION WITH HIGH PRANDTL NUMBER, INTERNATIONAL JOURNAL OF HEAT AND MASS TRANSFER. 134. 554-565

[36]OHK SEUNG-MIN, CHUNG BUM-JIN (2017), NATURAL CONVECTION HEAT TRANSFER INSIDE AN OPEN VERTICAL PIPE: INFLUENCES OF LENGTH DIAMETER AND PRANDTL NUMBER, INTERNATIONAL JOURNAL OF THERMAL SCIENCES. 115, 54-64

[37]ACHARYA, SWASTIK & AGRAWAL, SUMIT & DASH, SUKANTA. (2017). NUMERICAL ANALYSIS OF NATURAL CONVECTION HEAT TRANSFER FROM A VERTICAL HOLLOW

CYLINDER SUSPENDED IN AIR. JOURNAL OF HEAT TRANSFER. 140. 10.1115/1.4038478.

[38]TRITTON, D.J. (1988). *PHYSICAL FLUID DYNAMICS* (SECOND ED.). OXFORD UNIVERSITY PRESS

[39]ANSYS FLUENT 12.0 THEORY GUIDE. AVAILABLE: HTTPS://WWW.AFS.ENEA.IT/PROJECT/NEPTUNIUS/DOCS/FLUENT/HTML/TH/MAIN_PRE.HTM

[40]COLEMAN, HUGH & MEMBERS, COMMITTEE. (2009). ASME V&V 20-2009 STANDARD FOR VERIFICATION AND VALIDATION IN COMPUTATIONAL FLUID DYNAMICS AND HEAT TRANSFER (V&V20 COMMITTEE CHAIR AND PRINCIPAL AUTHOR).

APPENDICES

APPENDIX A: TEMPERATURE AND VELOCITY PROFILES

Q10

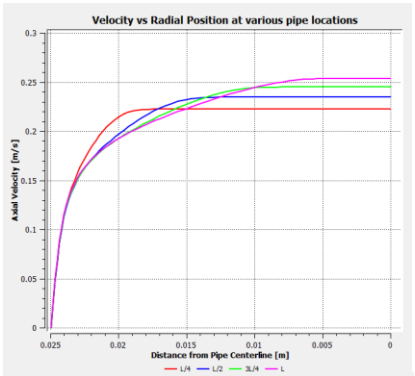

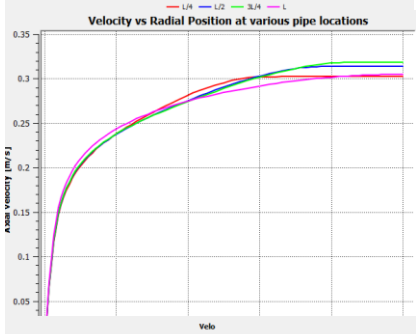

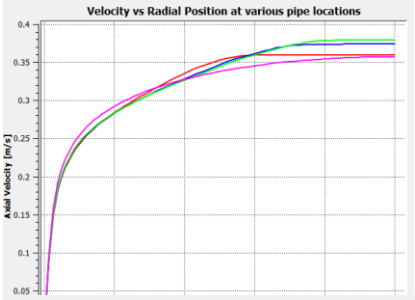

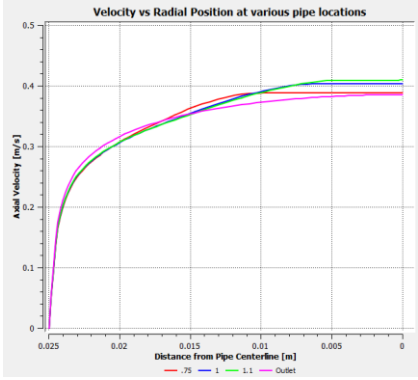

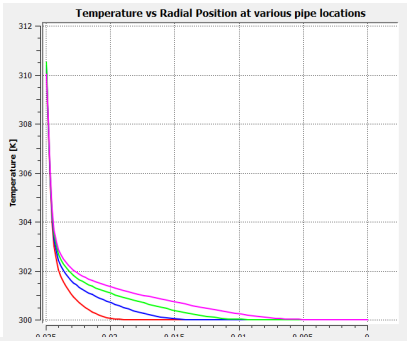

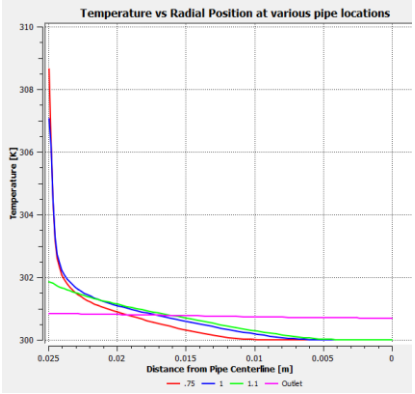

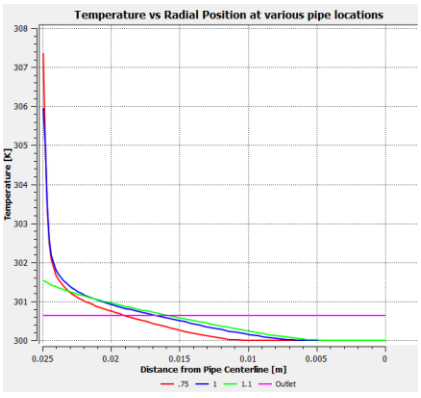

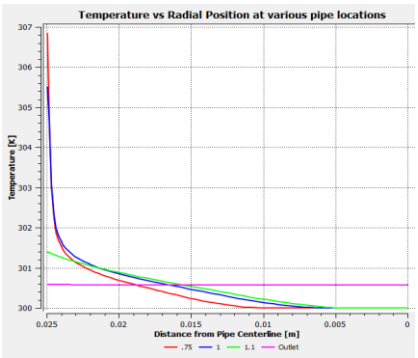

Q100

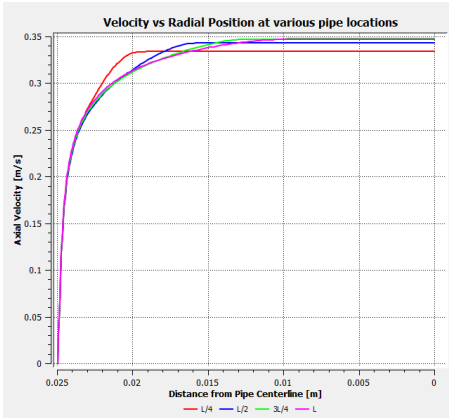
Velocity vs Radial Position at various pipe locations
Axial Velocity [m/s]
Distance from Pipe Centerline [m]
L/4
L/2
3L/4
L

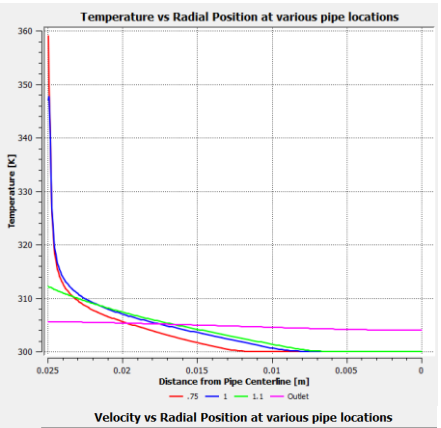
Temperature vs Radial Position at various pipe locations
Temperature [K]
Distance from Pipe Centerline [m]
.75
1
1.1
Outlet

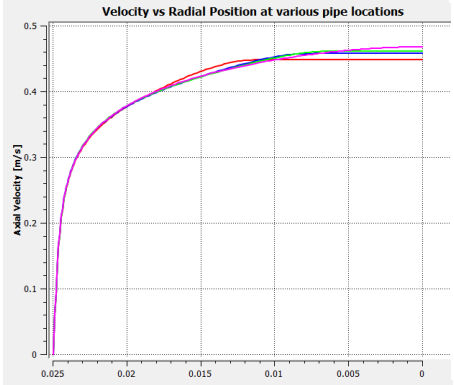
Velocity vs Radial Position at various pipe locations
Axial Velocity [m/s]
Distance from Pipe Centerline [m]

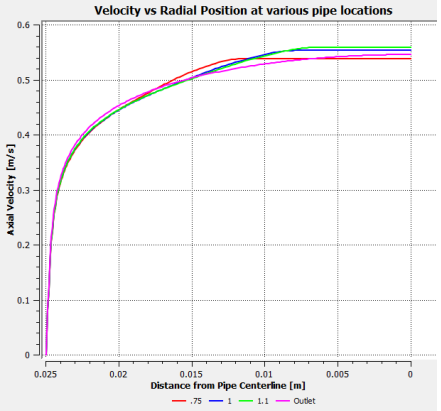
Velocity vs Radial Position at various pipe locations
Axial Velocity [m/s]
Distance from Pipe Centerline [m]
.75
1
1.1
Outlet

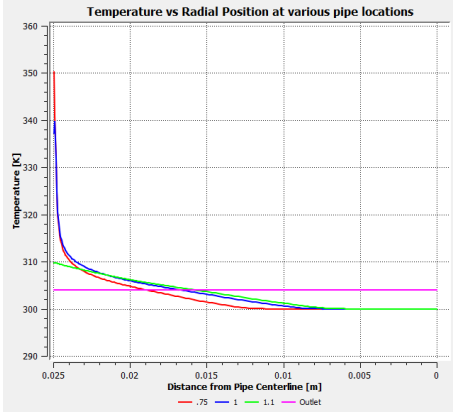
Temperature vs Radial Position at various pipe locations
Temperature [K]
Distance from Pipe Centerline [m]
.75
1
1.1
Outlet

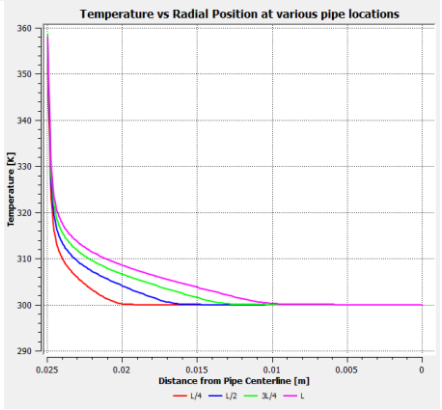
Temperature vs Radial Position at various pipe locations
Temperature [K]
Distance from Pipe Centerline [m]
L/4
L/2
3L/4
L

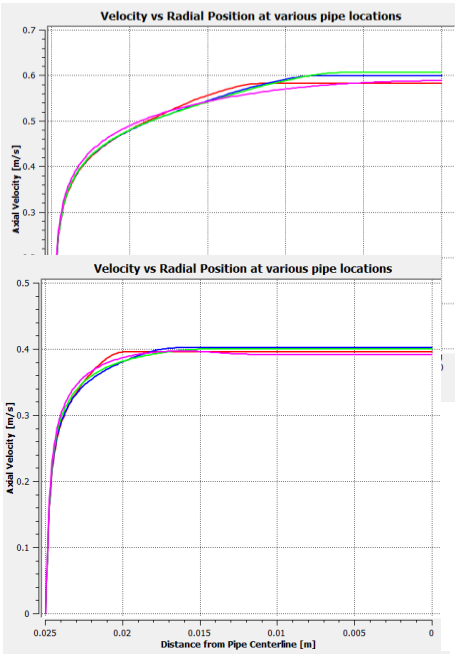
Velocity vs Radial Position at various pipe locations
Axial Velocity [m/s]
Distance from Pipe Centerline [m]

Velocity vs Radial Position at various pipe locations
Axial Velocity [m/s]
Distance from Pipe Centerline [m]

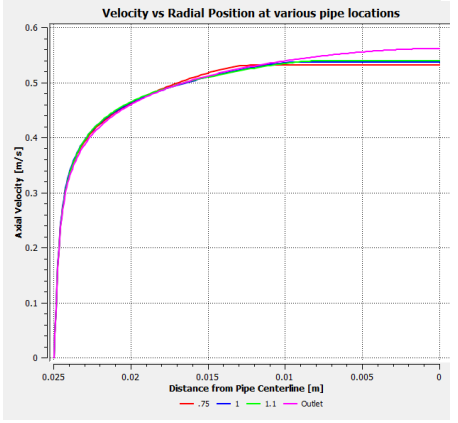
Velocity vs Radial Position at various pipe locations
Axial Velocity [m/s]
Distance from Pipe Centerline [m]
.75
1
1.1
Outlet

Q250

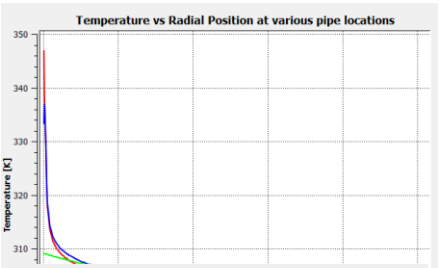
Temperature vs Radial Position at various pipe locations
Temperature [K]

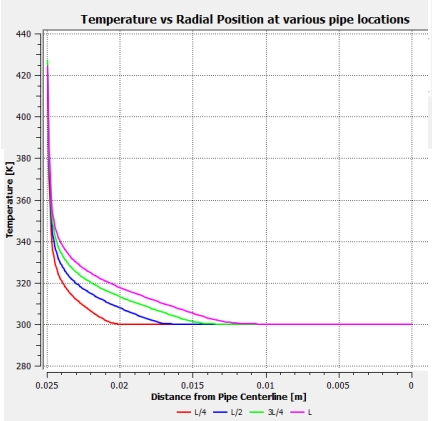
Temperature vs Radial Position at various pipe locations
Temperature [K]
Distance from Pipe Centerline [m]
L/4
L/2
3L/4
L

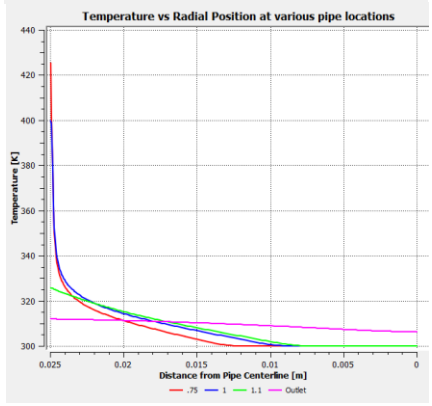
Temperature vs Radial Position at various pipe locations
Temperature [K]
Distance from Pipe Centerline [m]
.75
1
1.1
Outlet

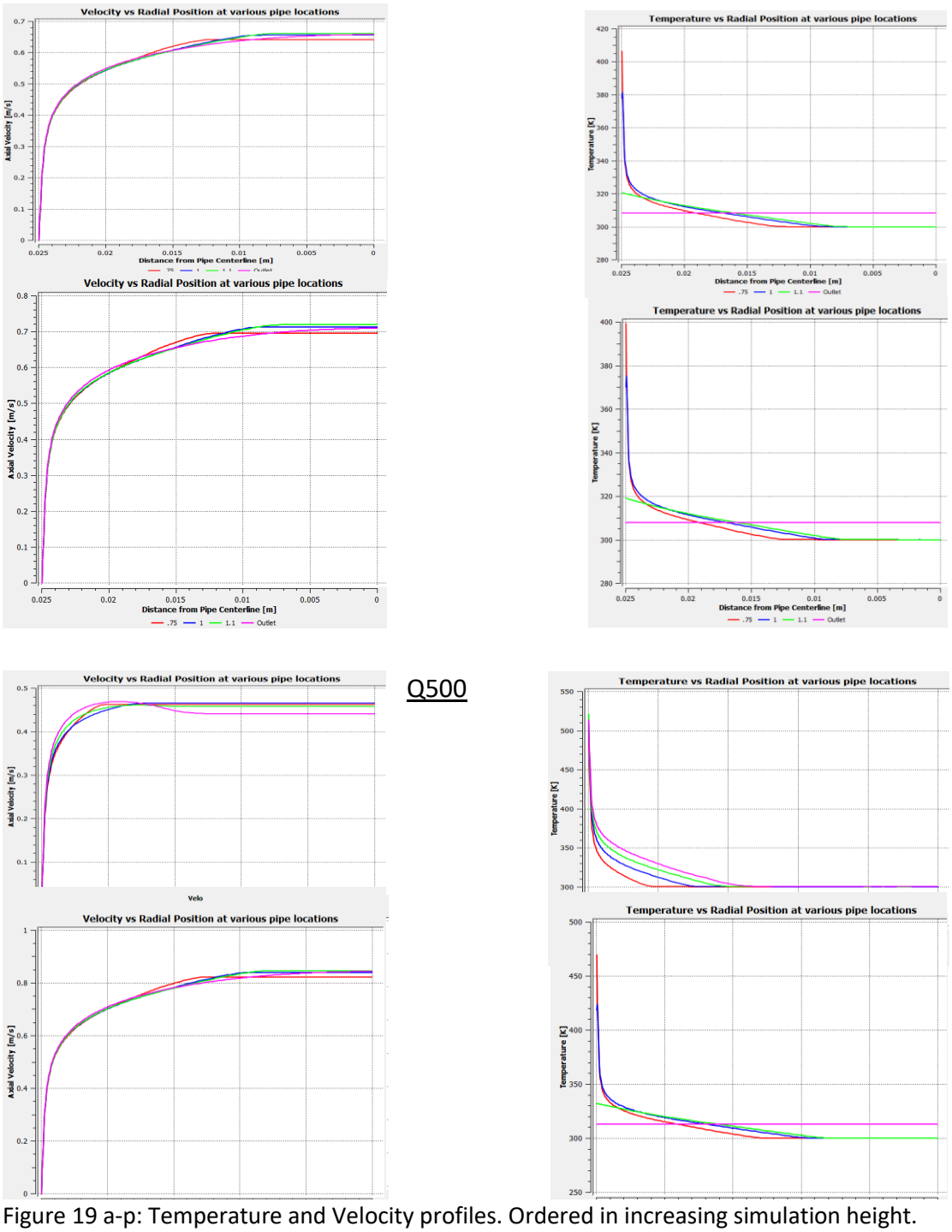

Figure 19 a-p: Temperature and Velocity profiles. Ordered in increasing simulation height.

APPENDIX B: HYDRODYNAMIC FORCE BALANCE

A 2-D hydrodynamic force balance was applied at the wall to analytically show the importance of the Rayleigh number. The control volume (CV) selected has one boundary at the wall and a constant radius (Figure 21). Only vertical motion is considered for this balance.

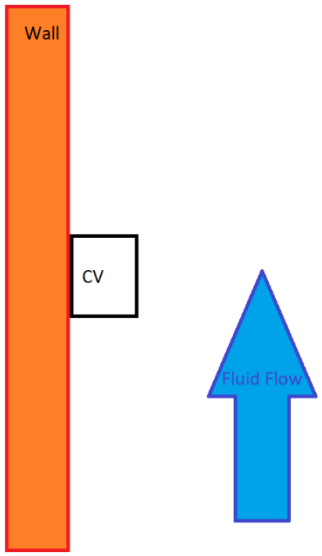

Figure 20: Representative CV

Begin with conservation of momentum on a control volume at steady state:

$$\sum F_{CV} = \sum \dot{m} V_{in} - \sum \dot{m} V_{out} = \sum F_{Pressure} + \sum F_{Body} + \sum F_{Viscous} + \sum F_{Other}$$

Next apply continuity:

$$\sum \dot{m}_{in} - \sum \dot{m}_{out} = \sum \rho A V_{in} - \sum \rho A V_{out} = 0$$

Assuming all flow enters form the bottom of the CV and leaves through the top, A becomes constant.

$$\sum \rho V_{in} - \sum \rho V_{out} = 0$$

Nest assume density does not change over the length of the CV. This assumption loses accuracy as the height of the CV is extended or the temperature differential is drastic. However, with a sufficiently small CV, the density does not have time to change and can therefore be considered constant. This yields:

$$\sum V_{in} - \sum V_{out} = 0 \rightarrow \sum V_{in} = \sum V_{out}$$

Combining this with conservation of momentum we find

$$\sum \dot{m} V_{in} - \sum \dot{m} V_{out} = 0 = \sum F_{Pressure} + \sum F_{Body} + \sum F_{Viscous} + \sum F_{Other}$$

We may now begin solving for each of the individual force terms on the right-hand side of the equation. The first term takes all pressure forces on the CV into account. There is no pressure in the vertical direction from the wall or the right side of the control volume. This term can therefore be written as:

$$\sum F_{Pressure} = F_{pressure\ bot} - F_{pressure\ top} = P_{bot} A_{bot} - P_{top} A_{top}$$

Recall that area is constant yielding

$$F_{pressure\ bot} - F_{pressure\ top} = P_{bot} - P_{top} = \Delta P$$

We may now define the body forces as force from gravity, generally written as

$$\sum F_{Body} = \rho g$$

The gravity term must now be modified to include the effects of changing density. While these effects were previously ignored, they are considered here per the Boussinesq approximation. The gravity force with buoyant effects is now defined as:

$$\sum F_{Body} = (\rho_0 + \Delta\rho)g - \rho_0 g = \Delta\rho g V$$

Further defining the $\Delta\rho$ term yields

$$\Delta\rho = \beta\rho_0\Delta T$$

$$\sum F_{Body} = \beta\rho_0\Delta T g V$$

Viscous forces are then defined as

$$\sum F_{Viscous} = -\mu\frac{du}{dy}A$$

Where h is the height of the CV. Breaking this into the viscous forces at each wall this term becomes

$$\sum F_{Viscous} = -\left(\mu\frac{du}{dy}|_{wall} + \mu\frac{du}{dy}|_{fluid}\right)A$$

There are no other forces of interest so the final term can be set to zero. Subbing all these back into the original equation yields

$$0 = \Delta P + \beta \rho_0 \Delta T g V \ - \left(\mu \frac{du}{dy}|_{wall} + \mu \frac{du}{dy}|_{fluid} \right) A$$

Rearrange

$$\Delta P * A = \beta \rho_0 \Delta T g V \ - \left(\mu \frac{du}{dy}|_{wall} + \mu \frac{du}{dy}|_{fluid} \right) A$$

Assume all dimensions of cube are identical

$$\Delta P h^2 = \beta \rho_0 \Delta T g h^3 \ - \left(\mu \frac{du}{dy}|_{wall} + \mu \frac{du}{dy}|_{fluid} \right) h^2$$

Assume that the height of the CV is sufficiently small so that $\Delta P \approx 0$

$$\beta \rho_0 \Delta T g h^3 = \left(\mu \frac{du}{dy}|_{wall} + \mu \frac{du}{dy}|_{fluid} \right) h^2$$

Assume $\frac{du}{dy}|_{fluid} = \frac{du}{dy}|_{wall}$

$$\beta \rho_0 \Delta T g h^3 = \left(\mu \frac{du}{dy}|_{wall} \right) h^2$$

Thermal diffusion occurs proportional to $\frac{\kappa}{r^2}$. Including these effects and rearranging yields

$$\frac{g \rho \beta \Delta T * h^4}{\mu \kappa} = r$$

Scaling the distance from the wall as an arbitrary factor (f) of h yields

$$\frac{g\rho\beta\Delta T * h^3}{\mu\kappa} = f$$

The left-hand side of this equation is the Rayleigh number, showing the relation between the Rayleigh number and the forces acting on the fluid in natural circulation scenarios. Note that the larger the driving head, the smaller the CV must be to be able to neglect the pressure term.